Monthly Notices of the ROYAL ASTRONOMICAL SOCIETY

MNRAS **478,** 2461–2479 (2018) doi:10.1093/mnras/sty1059
Advance Access publication 2018 April 26

Concurrent formation of supermassive stars and globular clusters: implications for early self-enrichment

Mark Gieles,[1]★ Corinne Charbonnel,[2,3] Martin G. H. Krause,[4] Vincent Hénault-Brunet,[5,6] Oscar Agertz,[7] Henny J. G. L. M. Lamers,[8] Nathan Bastian,[9] Alessia Gualandris,[1] Alice Zocchi[10,11] and James A. Petts[1]

[1]*Department of Physics, University of Surrey, Guildford GU2 7XH, UK*
[2]*Department of Astronomy, University of Geneva, Chemin des Maillettes 51, CH-1290 Versoix, Switzerland*
[3]*IRAP, UMR 5277, CNRS and Université de Toulouse, 14, avenue Édouard Belin, F-31400 Toulouse, France*
[4]*Centre for Astrophysics Research, School of Physics, Astronomy and Mathematics, University of Hertfordshire, College Lane, Hatfield AL10 9AB, UK*
[5]*National Research Council, Herzberg Astronomy & Astrophysics, 5071 West Saanich Road, Victoria, BC V9E 2E7, Canada*
[6]*Department of Astrophysics/IMAPP, Radboud University, PO Box 9010, NL-6500 GL Nijmegen, the Netherlands*
[7]*Lund Observatory, Department of Astronomy and Theoretical Physics, Lund University, Box 43, SE-221 00 Lund, Sweden*
[8]*Astronomical Institute Anton Pannekoek, University of Amsterdam, Science Park 904, NL-1098 XH Amsterdam, the Netherlands*
[9]*Astrophysics Research Institute, Liverpool John Moores University, 146 Brownlow Hill, Liverpool L3 5RF, UK*
[10]*Dipartimento di Fisica e Astronomia, Università degli Studi di Bologna, viale Berti Pichat 6/2, I-40127 Bologna, Italy*
[11]*European Space Research and Technology Centre, Keplerlaan 1, NL-2200 AG Noordwijk, the Netherlands*

Accepted 2018 April 23. Received 2018 April 23; in original form 2017 November 24

ABSTRACT

We present a model for the concurrent formation of globular clusters (GCs) and supermassive stars (SMSs, $\gtrsim 10^3$ M$_\odot$) to address the origin of the HeCNONaMgAl abundance anomalies in GCs. GCs form in converging gas flows and accumulate low-angular momentum gas, which accretes on to protostars. This leads to an adiabatic contraction of the cluster and an increase of the stellar collision rate. A SMS can form via runaway collisions if the cluster reaches sufficiently high density before two-body relaxation halts the contraction. This condition is met if the number of stars $\gtrsim 10^6$ and the gas accretion rate $\gtrsim 10^5$ M$_\odot$ Myr^{-1}, reminiscent of GC formation in high gas-density environments, such as – but not restricted to – the early Universe. The strong SMS wind mixes with the inflowing pristine gas, such that the protostars accrete diluted hot-hydrogen burning yields of the SMS. Because of continuous rejuvenation, the amount of processed material liberated by the SMS can be an order of magnitude higher than its maximum mass. This 'conveyor-belt' production of hot-hydrogen burning products provides a solution to the mass budget problem that plagues other scenarios. Additionally, the liberated material is mildly enriched in helium and relatively rich in other hot-hydrogen burning products, in agreement with abundances of GCs today. Finally, we find a super-linear scaling between the amount of processed material and cluster mass, providing an explanation for the observed increase of the fraction of processed material with GC mass. We discuss open questions of this new GC enrichment scenario and propose observational tests.

Key words: stars: abundances – stars: black holes – stars: kinematics and dynamics – supergiants – globular clusters: general – galaxies: star clusters: general.

1 INTRODUCTION

What started as a curiosity of the horizontal branch morphology of globular clusters (GCs) – the so-called 2$^{\rm nd}$ parameter problem (Sandage & Wildey 1967) – has become the largest unsolved problem of GC stellar populations. Nearly all old and massive GCs ($\gtrsim$10 Gyr, $\gtrsim 10^5$ M$_\odot$) display anticorrelated C–N and O–Na abundances (e.g. Carretta et al. 2009a, 2010a). A fraction of the GCs (preferentially the most massive and most metal-poor ones, with some exceptions) also display anticorrelated Mg–Al abundances (Carretta et al. 2009b; Mészáros et al. 2015; Pancino et al. 2017). Recently, Hollyhead et al. (2017) found spectroscopic evidence for

★ E-mail: m.gieles@surrey.ac.uk

N enhancement in the 8 Gyr old Small Magellanic Cloud (SMC) cluster Lindsay 1.

In addition to these spectroscopic peculiarities, most GCs present photometric signatures of the presence of multiple stellar populations (MSPs), e.g. broadened or multiple sequences in different areas of the colour–magnitude diagram (e.g. Anderson 2002; Bedin et al. 2004; Piotto et al. 2007, 2015; Milone et al. 2012, 2013; Martocchia et al. 2018). Using *Hubble Space Telescope* (*HST*) imaging in filters that are sensitive to C, N, and O variations, Niederhofer et al. (2017) found N enhancement in stars in three clusters with ages of 6–8 Gyr in the SMC. This was also found in the 2 Gyr old cluster NGC 1978 in the Large Magellanic Cloud (Martocchia et al. 2018). So far, no evidence for MSPs has been found in clusters younger than ∼2 Gyr (e.g. Mucciarelli et al. 2008; Cabrera-Ziri et al. 2015, 2016; Martocchia et al. 2018). There is currently no explanation for the origin of these ubiquitous MSPs in old star clusters, but the consensus is that a fraction of the GC stars contain products of hot-hydrogen burning (Prantzos, Charbonnel & Iliadis 2017), which, via the CNO-cycle ($\gtrsim$20 MK), the NeNa-chain ($\gtrsim$45 MK), and the MgAl-chain ($\gtrsim$70 MK), gives rise to anticorrelations between C–N, O–Na, and Mg–Al, respectively (Denisenkov & Denisenkova 1990; Langer, Hoffman & Sneden 1993; Ventura et al. 2001; Prantzos, Charbonnel & Iliadis 2007; Charbonnel 2016; Prantzos et al. 2017). The main-sequence broadening in optical filters is thought to be due to a spread in helium abundance (ΔY, with Y being the helium mass fraction; e.g. Norris 2004; D'Antona et al. 2005; Charbonnel 2016, and references therein).

Apart from a few exceptions – such as Omega Centauri (ω Cen) and M54, which are among the most massive clusters and may be (former) nuclear clusters – most GCs show no spread in iron abundance, meaning that enrichment from supernova explosions needs to be avoided. Finally, the maximum Na enhancement is similar in all GCs, but the ΔY varies from cluster to cluster (Bastian, Cabrera-Ziri & Salaris 2015). In this paper, we focus on these 'Fe-normal' GCs (the large majority) that show light element variations.

Three possible polluters that reach the required temperatures to explain the properties of these GCs have been put forward: asymptotic giant branch (AGB) stars (Ventura et al. 2001), massive stars ($\gtrsim$20 $M_\odot$, Maeder & Meynet 2006; Prantzos & Charbonnel 2006; de Mink et al. 2009), and supermassive stars (SMSs, $\gtrsim 10^3$ $M_\odot$; Denissenkov & Hartwick 2014). The models that try to explain the GC abundance anomalies and invoke AGB stars (massive enough to undergo hot-bottom burning; Ventura et al. 2001, 2013; D'Ercole et al. 2008) or fast-rotating massive stars (FRMS, i.e. main-sequence and luminous blue variable (LBV) massive stars rotating at or near critical speed; Decressin et al. 2007a; Krause et al. 2013) assume that a second generation of stars forms from the yields of a first generation. However, none of these sources is able to satisfy all the nucleosynthesis constraints (Bastian et al. 2015; Prantzos et al. 2017). AGB nucleosynthesis builds an O–Na correlation instead of the observed anticorrelation (Forestini & Charbonnel 1997; Denissenkov & Herwig 2003; Karakas & Lattanzio 2007; Siess 2010; Ventura et al. 2013; Doherty et al. 2014), and it releases He-burning products, thus predicting total C+N+O variations that are not observed in GCs (Karakas et al. 2006; Decressin et al. 2009, but see Yong, Grundahl & Norris 2015). On the other hand, the FRMS model predictions hardly reach Mg-burning temperature required to fit the observed Mg–Al anticorrelation without predicting strong He enrichment (Decressin et al. 2007a). Predicting the correct CNONaMgAl abundances without overpredicting ΔY is a general problem for all the polluters (Bastian et al. 2015), because recent results of *HST* photometry (e.g. Milone et al. 2015; Nardiello et al. 2015) show that ΔY is generally low. However, current SMS models with masses between $\sim 2 \times 10^3$ and 2×10^4 $M_\odot$ reach the required central temperature of ∼72−78 MK already at the very beginning of the evolution on the main sequence, when He enrichment is minute (Prantzos et al. 2017). Consequently, at that early evolution phase the H-burning products of SMSs show remarkable agreement with the various observed abundance anticorrelations (see fig. 1 in Denissenkov et al. 2015) and Mg isotopic ratios (Denissenkov & Hartwick 2014). As of today, SMS thus appear to be the most appealing candidate from the nucleosynthesis point of view, assuming that these fully convective objects release their entire material at the very beginning of the main sequence to avoid overproduction of He.

Getting the abundance patterns right is an important step, but a successful model for the origin of the abundance anomalies in GCs should also be able to explain how the required amount of material can be produced, and acquired by the low-mass stars that survive until today. Models that invoke a second burst of star formation from the yields of a first generation – hereafter referred to as multiple generation models (MGMs) – struggle to produce the required amount of processed material and need either a first generation with a top-heavy stellar initial mass function (IMF; Prantzos & Charbonnel 2006; Karakas et al. 2006), or need the cluster to lose $\gtrsim$90 per cent of the first generation of stars (Prantzos & Charbonnel 2006; D'Ercole et al. 2008; Schaerer & Charbonnel 2011) to end up with a significant fraction of polluted stars ($\gtrsim$50–90 per cent as observed in the most massive GCs). The latter scenario makes strong predictions for the fraction of stars in GCs relative to the field, which is in tension with empirical estimates of this (high) ratio in dwarf galaxies (Larsen, Strader & Brodie 2012; Larsen et al. 2014). Additionally, common stellar feedback processes are not able to achieve this via gas expulsion (Krause et al. 2012) and need careful fine tuning to avoid the cluster to disperse completely (Decressin et al. 2010; Khalaj & Baumgardt 2015). Finally, relying on internal processes to expel a large amount of pristine stars generally leads to a decrease in the remaining fraction of polluted stars with GC mass (Bastian & Lardo 2015), which is not observed. In fact, both the inferred ΔY and the fraction of polluted stars ($f_{\rm poll}$) correlate with GC mass (Milone et al. 2014, 2017). These trends imply that more polluted material is required per unit of cluster mass in massive GCs, requiring fine tuning in MGMs (for recent reviews, see Renzini et al. 2015; Charbonnel 2016; Bastian 2017; Bastian & Lardo 2018). The inability of any existing MGM to create sufficient polluted material and produce the correct trends with GC mass, is commonly referred to as the 'mass budget problem'.

Given the challenges with the MGMs, a model requiring only a single generation of stars is therefore more attractive. Bastian et al. (2013) present such a scenario, in which low-mass pre-main-sequence stars with large discs sweep up polluted material released by interacting, massive binary stars. However, full mixing of the polluted material with the proto-stellar seeds is required to explain all the abundance patterns, which requires that the accretion occurs at the very beginning of the pre-main sequence when the contracting stars are still entirely convective, i.e. on time-scales shorter than ∼1–3 Myr (Salaris & Cassisi 2014; D'Antona et al. 2014). In addition, accretion of hot and tenuous, low-angular momentum gas on a disc causes the disc to rapidly shrink and accrete on the star, thereby limiting the cross-section for further accretion (Wijnen et al. 2016). This early disc accretion is therefore not efficient enough to explain the amount of pollution that is observed. Alternatively, Charbonnel et al. (2014) propose that only massive stars formed out of pristine GC material, and that only low-mass stars formed from contami-

nated gas in the immediate vicinity of the FRMS polluters during their very short lifetime (∼3–8 Myr). Assuming 100 per cent recycling of the FRMS ejecta and accounting for dilution as required to explain the presence of Li in polluted stars, the mass initially locked in the massive star polluters should have been only two to four times the present-day stellar mass, which strongly alleviates the mass budget problem. Nevertheless, the required IMF is contrived and this idea does not give rise to the observed trends with GC mass.

Because of the promising results of the SMS yields and the problems with the MGMs (Renzini et al. 2015; Charbonnel 2016; Bastian 2017; Bastian & Lardo 2018), we here search for a solution in which a SMS forms simultaneously with the GC and immediately pollutes the cluster gas and eventually low-mass protostars during the cluster formation process, i.e. without relying on multiple starbursts. We focus in particular on overcoming the mass budget problem, and understanding the observed correlations of ΔY and $f_{\rm poll}$ with GC mass and the relative abundances of CNONaMgAl and He. Because the MSP phenomenon is found in GCs with different [Fe/H], the formation of the SMS cannot rely on inefficient gas cooling in metal-free initial conditions, as invoked in models of the formation of massive Population III stars (e.g. Abel, Bryan & Norman 2002; Regan & Haehnelt 2009). Instead, the model presented in this work relies on the stellar dynamical behaviour of proto-clusters in the gas accretion phase, i.e. physics that is largely independent of metallicity (but see Sections 3.3 and 4.10 for a discussion on metallicity dependence). Several of the ingredients of the dynamical model are based on the theoretical work by Bonnell, Bate & Zinnecker (1998) and Clarke & Bonnell (2008), and the numerical work by Davis, Clarke & Freitag (2010) and Moeckel & Clarke (2011). These studies discuss the relative importance of gas accretion and stellar collisions in massive star formation. In this work, we push this into the regime of GCs and show that this is where SMSs can form via stellar collisions. We also provide scaling relations for the dependence of the mass of the SMS on cluster mass.

In Section 2, we present a framework for the formation of a SMS during GC formation. In Section 3, we use this new SMS formation model to put forward a new GC self-enrichment scenario to explain the observed abundance anomalies of light elements (HeCNONaMgAl) in Fe-normal GCs. In Section 4, we discuss the model uncertainties and predictions and observational tests that can verify this scenario. Our conclusions are given in Section 5.

2 SMS FORMATION DURING GC FORMATION

In this section, we introduce a simple model for the formation of a SMS via stellar collisions during GC formation. We consider the effect of gas accretion and subsequent contraction of the cluster, collisions between stars and the effect of two-body relaxation. We derive the condition for SMS formation and scaling relations for the rate of growth of the SMS. In Section 3, we add the mass-loss from the SMS as the result of a stellar wind.

2.1 Typical initial conditions

Consider the very first phases of star formation in dense and turbulent molecular clumps, in which a proto-stellar core mass function with a slope close to the Salpeter value (Salpeter 1955) develops via gravoturbulent fragmentation (Padoan & Nordlund 2002; Hennebelle & Chabrier 2008) and/or competitive accretion (Zinnecker 1982; Bonnell et al. 1998; Ballesteros-Paredes et al. 2015). Protostars form quickly (less than a core free-fall time) from a seed mass (Guszejnov & Hopkins 2015), which then continues accreting from the global mass reservoir and/or their local collapsing cores. The protostars form with a mass spectrum, and have typical initial masses of[1] $m_0 \simeq 0.1\,{\rm M}_\odot$ and radii of $r_0 \simeq 3\,{\rm R}_\odot$ (e.g. Tout, Livio & Bonnell 1999; Hartmann, Herczeg & Calvet 2016). Clusters form with a range of masses and densities, but typical values we consider are initial stellar densities within the half-mass radius ($R_{\rm h0}$) of $\rho_{\rm h0} \simeq 10^3\,{\rm M}_\odot/{\rm pc}^3$, such that a proto-cluster with a stellar mass of $M_0 \simeq 10^5\,{\rm M}_\odot$ has a radius of $R_{\rm h0} \simeq 2.3\,{\rm pc}$. The total number of stars is then $N = M_0/m_0 = 10^6$. Initially, the velocities of the stars are set by the turbulent velocities in the cloud and the gas potential. Subclusters of protostars quickly virialize in their own potentials, because the local star formation efficiency is high (Moeckel et al. 2012) and the subclusters contract as the result of gas accretion and merge with each other to become a dense, self-gravitating stellar system surrounded by lower density gas (Moeckel & Clarke 2011). The resulting dynamical time of the virialized proto-cluster is $\tau_{\rm dyn0} \sim (G M_0/R_{\rm h0}^3)^{-1/2} \simeq 0.16\,{\rm Myr}$, with G the gravitational constant. From here on we consider the cluster to be a single entity, but we get back to the possible importance of subclustering in the discussion (Section 4.5). In the next section, we discuss the evolution of the stellar cluster after gas accretion on its member stars has commenced.

2.2 Gas accretion and adiabatic contraction

After the protostars formed, they grow in mass by accretion of gas (e.g. Bonnell et al. 1998; Krumholz et al. 2009; Hartmann et al. 2016; Vázquez-Semadeni, González-Samaniego & Colín 2017). We assume that this gas accretion is fuelled by gas flowing into the cluster with 100 per cent accretion efficiency and that no new stars form (i.e. N remains constant).[2] We define the gas accretion time-scale as

$$\tau_{\dot{M}} = \frac{M}{\dot{M}}, \tag{1}$$

where $\dot{M}$ is the gas accretion rate on to the cluster and M is the instantaneous total mass in stars. We assume that $\dot{M}$ is constant in time, such that M and $\tau_{\dot{M}}$ increase linearly with time during the accretion phase. This is different from what is found in models of the collapse of a self-gravitating cloud ($\dot{M} \propto t$, Murray & Chang 2015), but a roughly constant $\dot{M}$ in time (or slightly declining with time) was found by Li et al. (2017) in cosmological zoom-in simulations, where the accretion rate is regulated by stellar feedback. In our model, $\dot{M}$ is a free parameter and we assume that $\dot{M}$ is proportional to N, i.e. $\dot{M} = \langle \dot{m}_{\rm acc} \rangle N$, where $\langle \dot{m}_{\rm acc} \rangle$ is the average accretion rate on individual stars. Our assumption of $\dot{M} \propto N$ means that $\langle \dot{m}_{\rm acc} \rangle$ does not depend on N. To preserve the shape of the stellar mass function and keep the total $\dot{M}$ constant we assume that $\dot{m}_{\rm acc}$ is proportional to the initial mass of the star (i.e. $\dot{m}_{\rm acc} \propto m_0$).[3] We assume a typical value of $\langle \dot{m}_{\rm acc} \rangle \simeq 0.1\,{\rm M}_\odot\,{\rm Myr}^{-1}$, which is similar to what is found for young, low-mass pre-main-sequence stars in the

[1] From hereon we denote all quantities with subscripts 0 when referring to their value at the start of gas accretion and we use capital symbols for the cluster quantities and lower case symbols for those of the stars and the SMS.
[2] It does not matter for the response of the cluster whether the gas accretes on the stars, or on the molecular clumps (i.e. before the collapse).
[3] This is not a critical assumption to approximately preserve the IMF slope, because for Bondi–Hoyle accretion (i.e. $\dot{m}_{\rm acc} \propto m^2$) the mass function evolves to a −2 power law, i.e. close to Salpeter, independent of the initial functional form (Zinnecker 1982; Ballesteros-Paredes et al. 2015).

Milky Way ($\sim 10^5$ yr, $\sim 0.7\,\mathrm{M}_\odot$, Hartmann, Herczeg & Calvet 2016; De Marchi, Panagia & Beccari 2017) and in magnetohydrodynamic simulations (e.g. Offner & Chaban 2017). For this accretion rate, the initial accretion time-scale is $\tau_{\dot{M}0} \simeq 1$ Myr, which is reasonable given our current understanding of GC formation time-scales (i.e. few Myr, see e.g. Kimm et al. 2016; Li et al. 2017; Kim et al. 2018). For these values of the accretion rate, the mean mass of stars grows to $0.6\,\mathrm{M}_\odot$ in 5 Myr, roughly equal to the mean mass of a Kroupa (2001) IMF (in the range 0.1–100 $\mathrm{M}_\odot$). We assume that the accretion is halted at this time by stellar feedback (Li et al. 2017). We discuss the duration of the accretion phase and the start of the stellar evolution phase in more detail in Section 3.1.

For the adopted typical value of $\tau_{\dot{M}}$, we have $\tau_{\dot{M}} \gg \tau_{\rm dyn}$, such that the angular momentum of stars plus gas is conserved during the accretion and the stellar clusters responds adiabatically. We define $V_{\rm rms}$ as the one-dimensional velocity dispersion of the cluster, and assume that the angular momentum of the inflowing gas is negligible, such that the adiabatic invariant $MV_{\rm rms}R_{\rm h}$ of the star cluster is preserved, while M increases as the result of accretion (Blumenthal et al. 1986). Because $\tau_{\dot{M}} \gg \tau_{\rm dyn}$, virial equilibrium is maintained and then $V_{\rm rms} \simeq \sqrt{GM/(6R_{\rm h})}$ and we find that the star cluster contracts as $R_{\rm h} \propto M^{-3}$ (Bonnell et al. 1998). From this we see that the gas accretion process leads to a rapid increase of the density ($\rho_{\rm h} \propto M^{10}$), and stellar collisions can become important already after a modest amount of gas accretion (Moeckel & Clarke 2011).

The increasing density also leads to a decrease in the two-body relaxation time-scale. When this time-scale becomes shorter than $\tau_{\dot{M}}$, two-body heating becomes important and the cluster starts expanding (Clarke & Bonnell 2008), reducing the collision rate. When these two time-scales are of comparable magnitude, the cluster has reached its maximum density and a requirement for SMS formation is thus that sufficient stellar collisions need to happen before this moment. To quantify this condition, we need a measure of the relaxation time-scale, for which we use the definition of the half-mass relaxation time-scale from Spitzer & Hart (1971)

$$\tau_{\rm rh} \simeq 0.138 \frac{N}{\psi \ln\Lambda}\left(\frac{R_{\rm h}^3}{GM}\right)^{1/2}. \quad (2)$$

Here, $\ln\Lambda$ is the Coulomb logarithm and ψ depends on the stellar mass spectrum: $\psi = 1$ for equal-mass clusters and $\psi \simeq 10-100$ for clusters with a full mass spectrum (Gieles et al. 2010). We adopt a constant $\ln\Lambda = 10$ and we assume $\psi = 30$ to include the effect of a spectrum of masses for the accreting protostars.

For a constant N and the scaling $R_{\rm h} \propto M^{-3}$, we find $\tau_{\rm rh} \propto M^{-5}$ from equation (2). Combined with a constant $\dot{M}$, we have $\tau_{\rm rh}/\tau_{\dot{M}} \propto M^{-6}$. The maximum cluster density is reached when $\tau_{\dot{M}} \simeq N_{\rm rel}\tau_{\rm rh}$, with $N_{\rm rel} \simeq 10$ being the number of relaxation times that needs to elapse before collisional dynamics becomes important (see e.g. Cohn 1980 for the idealized case of a single-mass cluster and Alexander et al. 2014 for multimass clusters). From the linear increase of $M(t)$ and the relations for $\tau_{\rm rh}$ and $\tau_{\dot{M}}$ we find that the end of the contraction phase is at time

$$t_{\rm contr} = \tau_{\dot{M}0}\left[\left(\frac{N_{\rm rel}\tau_{\rm rh0}}{\tau_{\dot{M}0}}\right)^{1/6} - 1\right]. \quad (3)$$

We note that $t_{\rm contr}$ is also the time that $N_{\rm rel}$ half-mass relaxation time-scales have elapsed (i.e. $N_{\rm rel} = \int_0^{t_{\rm contr}} {\rm d}t'/\tau_{\rm rh}(t')$), hence $t_{\rm contr}$ can be thought of as the moment of core collapse. Because $t_{\rm contr}$ is more sensitive to $\tau_{\dot{M}0}$ than to $\tau_{\rm rh0}$, the start of the relaxation dominated phase is triggered by gas accretion and $t_{\rm contr}$ is therefore much shorter than the conventional core collapse of GCs, which happens on a time-scale of Gyr.[4]

At $t_{\rm contr}$, the total mass in stars has increased to (Davis et al. 2010)

$$M(t_{\rm contr}) = M_0\left(\frac{N_{\rm rel}\tau_{\rm rh0}}{\tau_{\dot{M}0}}\right)^{1/6}. \quad (4)$$

For the initial parameters of our fiducial cluster (Section 2.1) we have $\tau_{\rm rh0} \simeq 75$ Myr and combined with $\tau_{\dot{M}0} \simeq 1$ Myr (Section 2.2) we find that the mass needs to increase by only a factor of ~ 3 before two-body relaxation becomes important. The corresponding $t_{\rm contr} \simeq 2$ Myr, which is before feedback from supernova explosions becomes important, implying that the maximum density is reached before gas accretion stops. The weak dependence on $\tau_{\rm rh0}$ means that $t_{\rm contr}$ is relatively insensitive to N. The next question is whether stellar collisions can become important before two-body relaxation stops the contraction of the cluster. Before we address this, we first introduce the properties of the SMS in the next section.

2.3 SMS properties

To be able to follow the growth of the SMS, we need to know how its radius depends on its mass. The mass–radius relation for SMSs is very uncertain, but we can be guided by our understanding of massive stars. Crowther et al. (2010) present parameters for a sample of stars with masses $\sim 90-130\,\mathrm{M}_\odot$, and find that they have radii of $\sim 30\,\mathrm{R}_\odot$. We adopt a mass–radius relation of the form

$$r_{\rm SMS} = 30\,\mathrm{R}_\odot\left(\frac{m_{\rm SMS}}{100\,\mathrm{M}_\odot}\right)^{\delta}, \quad (5)$$

where $0 < \delta \lesssim 1$ for $m_{\rm SMS} > 100\,\mathrm{M}_\odot$ and $\delta = 0.5$ for $m_{\rm SMS} < 100\,\mathrm{M}_\odot$. Smoothed particle hydrodynamics (SPH) models of stellar collisions of solar-type stars show that the collision product is typically a factor 3–20 larger than a star with the same mass that started unperturbed (Lombardi et al. 2003). SPH models of colliding massive stars ($\gtrsim 100\,\mathrm{M}_\odot$) show that right after the collision the star can be 10–100 times larger than the equilibrium $r_{\rm SMS}$, and that the star settles to a radius that is a few times the equilibrium value after $\sim 10^3$ yr (Suzuki et al. 2007). The collision rate can be high enough to have the next collision occurring before this settling occurs. However, it is not clear how efficient a diffuse halo of a few $10^3\,\mathrm{R}_\odot$ is in dragging other stars into the SMS. We note that collisions and the high radiation pressure of stars $\gtrsim 300\,\mathrm{M}_\odot$ may lead to larger radii (Gräfener, Owocki & Vink 2012; Szécsi et al. 2015; Rob Izzard, private communication) and we consider the uncertain radii by varying δ.

The luminosity of a SMS, $l_{\rm SMS}$, is close to its Eddington limit for electron scattering: $l_{\rm Edd}/\mathrm{L}_\odot = 3.7 \times 10^4\, m_{\rm SMS}/\mathrm{M}_\odot$. The stellar models of Nadyozhin & Razinkova (2005) show that $\Gamma = l_{\rm SMS}/l_{\rm Edd}$ varies between 0.56 and 0.94 in the range of $3 \times 10^2 < m_{\rm SMS}/\mathrm{M}_\odot < 10^4$ and we adopt $\Gamma = 0.75$ such that

$$l_{\rm SMS} \simeq 2.8 \times 10^6\,\mathrm{L}_\odot\,\frac{m_{\rm SMS}}{100\,\mathrm{M}_\odot}. \quad (6)$$

This agrees well with the observed values from Crowther et al. (2010), who find luminosities of $(1.5-3) \times 10^6\,\mathrm{L}_\odot$. This is also in

[4]The reason that another core collapse occurs on this long time-scale is because after ~ 3 Myr the cluster expands by a factor of a few as the result of stellar mass-loss, thereby increasing $\tau_{\rm rh}$, and secondly because the massive stars die, such that ψ reduces to $\psi \simeq 2$ (Kim, Lee & Goodman 1998), which also increases $\tau_{\rm rh}$ (see equation 2). For a more elaborate discussion on core collapse(s) in multimass systems we refer to Breen & Heggie (2012, 2013).

good agreement (by a factor 2–3) with the luminosity of the zero-age main-sequence SMS models that we use for the nucleosynthesis discussion in Section 4.2 and that were computed by Denissenkov (private communication) with the evolution code MESA (Paxton et al. 2011) with the same assumptions as in Denissenkov et al. (2015).

With the Stefan–Boltzmann law (i.e. assuming blackbody radiation), the mass–radius relation (equation 5) and the luminosity (equation 6) we find that $T_{\rm eff} \simeq 43\,{\rm kK}\,(m_{\rm SMS}/100\,{\rm M}_\odot)^{1/4-\delta/2}$. This $T_{\rm eff}$ is in excellent agreement with what was found by Crowther et al. (2010) for unperturbed massive stars (∼40 kK). The δ-dependence implies that the SMS has a mass-independent $T_{\rm eff}$ for $\delta = 0.5$ and that SMSs are cooler than $100\,{\rm M}_\odot$ stars for $\delta > 0.5$.

Finally, we adopt an initial $m_{\rm SMS} = 5\,{\rm M}_\odot$ before gas accretion, which has a radius of $6.7\,{\rm R}_\odot$. With a description for the mass–radius relation in place, we can now proceed with the growth of the SMS via collisions.

2.4 Mass growth of a central SMS

The collision rate, $\dot{N}_{\rm coll}$, experienced by a star with mass $m_{\rm SMS}$ and $r_{\rm SMS}$ in a system with stellar number density n and velocity dispersion $V_{\rm rms}$, with other stars of mass m and radius r is (Hills & Day 1976; Binney & Tremaine 2008, Chapter 7)

$$\dot{N}_{\rm coll} = 2\sqrt{2\pi}\left(\frac{m_{\rm SMS}+m}{m_{\rm SMS}}\right)^{1/2} n V_{\rm rms} d^2 \left(1+\frac{G m_{\rm SMS}}{d V_{\rm rms}^2}\right), \qquad (7)$$

where it is assumed that a collision occurs when the stars are at a distance $d = r + r_{\rm SMS}$. The final term within brackets has two contributions: the first one is due to the geometrical cross-section of the star, and the second contribution is due to gravitational focusing, which enhances the cross-section of stars. For stellar collisions, the gravitational focusing term dominates, because the escape velocity from the stellar surface is much larger than the typical velocities of the stars, and therefore $G m_{\rm SMS}/(d V_{\rm rms}^2) \gg 1$. Davis et al. (2010) assumed that all stars have the same mass and radius to derive the total number of collisions in the contraction phase: $N_{\rm coll}(t_{\rm contr}) \propto N^{5/3}\dot{M}^{2/3}$. The number of collisions per star is a factor N smaller. Combined with our assumption that $\dot{M} \propto N$, we find that the number of collisions experienced by an individual star scales as $\propto N^{4/3}$. This super-linear scaling of $N_{\rm coll}$ with N shows that the stellar collisions experienced by a star in the adiabatic contraction phase are more important per unit of cluster mass in more massive clusters. Combined with the absence of a dependence on any other parameters, this is the first ingredient to explain the observed increase of $f_{\rm poll}$ and ΔY with GC mass (Section 3).

After a collision between two stars, the collision product is more massive and has a larger radius, which increases its cross-section and collision rate (see equation 7). There is therefore a high probability that the first collision product is involved in subsequent collisions and typically one very massive star forms as the result of stellar collisions ($\gtrsim$100 $\rm M_\odot$, e.g. Portegies Zwart & McMillan 2002; Portegies Zwart et al. 2004; Freitag, Gürkan & Rasio 2006; Mapelli 2016). To understand how the mass of a star grows as the result of continuous collisions, we assume that $m_{\rm SMS} \gg m$ and $r_{\rm SMS} \gg r$, which is true after several collisions, and with $\dot{m}_{\rm SMS}^{\rm coll} = \langle m\rangle \dot{N}_{\rm coll}$ we then see from equation (7) that the growth rate is

$$\dot{m}_{\rm SMS}^{\rm coll} \simeq 2\sqrt{2\pi}\, G\, m_{\rm SMS} r_{\rm SMS} \frac{\rho_{\rm c}}{V_{\rm rms}}, \qquad (8)$$

where $\rho_{\rm c}$ is the central mass density of the cluster, which we relate to $\rho_{\rm h}$ as $\rho_{\rm c} = f_{\rm ch}\rho_{\rm h}$, with[5] $f_{\rm ch} = 10^3$. Note that the dependence of $\dot{m}_{\rm SMS}^{\rm coll}$ on the central mass density means that a star in a mass segregated cluster, with a similar $\rho_{\rm c}$ and $V_{\rm rms}$, experiences the same $\dot{m}_{\rm SMS}^{\rm coll}$, as the result of fewer collisions with more massive stars. Defining the time-scale for the growth of the SMS as $\tau_{\dot{m}_{\rm SMS}} \equiv m_{\rm SMS}/\dot{m}_{\rm SMS}^{\rm coll}$, we have

$$\tau_{\dot{m}_{\rm SMS}} = \frac{1}{2\sqrt{2\pi}\, G\, r_{\rm SMS}} \frac{V_{\rm rms}}{\rho_{\rm c}}. \qquad (9)$$

In a contracting cluster, the ratio $V_{\rm rms}/\rho_{\rm c} \propto M^{-8}$, strongly reducing $\tau_{\dot{m}_{\rm SMS}}$ while the cluster grows in mass. For the properties of our initial conditions (i.e. when the contraction starts, Section 2.1) this time-scale is $\tau_{\dot{m}_{\rm SMS}0} \simeq 1680\,{\rm Myr}$ for a star of $5\,{\rm M}_\odot$ and radius $6.7\,{\rm R}_\odot$, i.e. collisions are irrelevant at the time of fragmentation and it reduces to $\lesssim$1 Myr after the cluster mass has increased by a factor of two. In addition, $\tau_{\dot{m}_{\rm SMS}}$ becomes shorter as collisions proceed, because $r_{\rm SMS}$ increases (for $\delta > 0$ in equation 5). In this section, we ignore the dynamical feedback of binaries on the cluster properties, which we discuss in Section 2.5. Then, a runaway collision process can occur and from integrating equation (8) we find that the time when $m_{\rm SMS} \to \infty$ is

$$t_\infty \simeq \tau_{\dot{M}0}\left[\left(\frac{9\tau_{\dot{m}_{\rm SMS}0}}{\delta\tau_{\dot{M}0}}\right)^{1/9} - 1\right]. \qquad (10)$$

This relation holds for $\tau_{\dot{m}_{\rm SMS}0}/\tau_{\dot{M}0} \gg 1$, which is satisfied because for the typical parameters of Section 2.1 we have $\tau_{\dot{m}_{\rm SMS}0}/\tau_{\dot{M}0} \simeq 700$. For a cluster to be able to form a SMS via stellar collisions, this runaway process needs to occur before the end of the contraction phase derived in Section 2.2, i.e. $t_\infty \lesssim t_{\rm contr}$. Using the expression for the end of the contraction phase in equation (3) we find that this criterion is met when

$$N \gtrsim 1.4\times10^6 \left(\frac{\dot{M}}{1.4\times10^5\,{\rm M}_\odot\,{\rm Myr}^{-1}}\right)^{-3/4} F_0, \qquad (11)$$

where F_0 depends on the initial conditions of the cluster, the protostars, and the SMS (see Section 2.1)

$$F_0 = \left(\frac{\psi}{30}\right)^{9/4}\left(\frac{N_{\rm rel}}{10}\right)^{-9/4}\left(\frac{\delta}{0.5}\right)^{-3/2}\left(\frac{f_{\rm ch}}{10^3}\right)^{-3/2} \times \left(\frac{\rho_{\rm h0}}{10^3\,{\rm M}_\odot\,{\rm pc}^{-3}}\right)^{-1/8}\left(\frac{m_0}{0.1\,{\rm M}_\odot}\right)^{5/4}\left(\frac{r_{\rm SMS0}}{6.7\,{\rm R}_\odot}\right)^{-3/2}, \qquad (12)$$

where the adopted scaling $r_{\rm SMS0} = 6.7\,{\rm R}_\odot$ applies to $m_{\rm SMS0} = 5\,{\rm M}_\odot$ (see Section 2.3). From equation (11) we see that in the GC mass regime ($M \gtrsim$ few $\times 10^5\,{\rm M}_\odot$), a runaway stellar collision process occurs before the contraction phase ends. The criterion is surprisingly insensitive to $\rho_{\rm h0}$, implying that N is the dominant cluster property determining whether a runaway collision can occur. Apart from $\dot{M}$, all other parameters are similar in different environments, making $\dot{M}$ the only environmental parameter. From this simple argument we see that massive (i.e. high N) clusters in environments with high gas accretion rates (i.e. high $\dot{M}$) are the places in which runaway collisions can take place to form a SMS. At high redshift, the high gas densities and gas fractions enable the formation of massive GCs (Elmegreen & Efremov 1997). These conditions also lead to higher accretion rates compared to the present day (Elmegreen 2017; Li

[5]This density contrast depends on the density profile of the cluster, for which we have little guidance. For a King (1966) model with dimensionless central potential of $W_0 = 9(10)$ it is roughly $f_{\rm ch} = 440(2000)$.

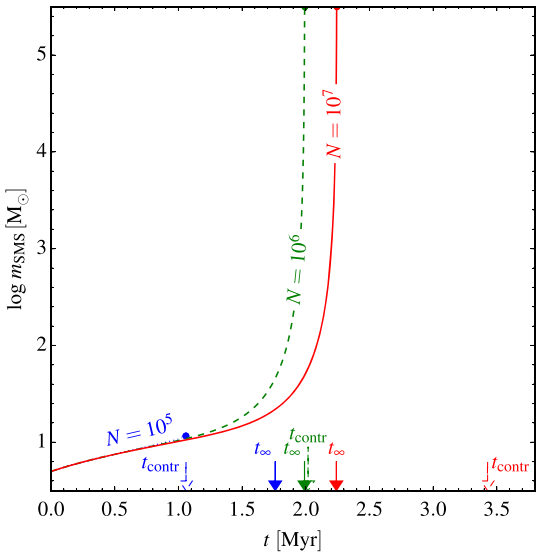

Figure 1. The mass of a SMS that grows by gas accretion and stellar collisions in the centre of a gas accreting cluster, for clusters with different N. The values of $m_{\rm SMS}(t)$ are found by numerically integrating $\dot{m}_{\rm SMS} = \dot{m}_{\rm acc} + \dot{m}^{\rm coll}_{\rm SMS}$, with $\dot{m}_{\rm acc} = m_{\rm SMS0}\,{\rm Myr}^{-1}$ and $\dot{m}^{\rm coll}_{\rm SMS}$ given by equation (8). Lines are plotted until $t = \min(t_{\rm contr}, t_\infty)$ and the effect of relaxation is not included. The end of the contraction phases ($t_{\rm contr}$) are also indicated and from this it can be seen that runaway collisions do not occur in clusters with $N \lesssim 10^6$, because for those clusters $t_{\rm contr} < t_\infty$, while $t_{\rm contr} > t_\infty$ for the larger clusters and runaway collisions occur before the end of the contraction phase.

et al. 2017). At this stage, we have the first quantitative explanation for why SMS formation occurred predominantly in massive, old GCs.

In Fig. 1, we show the evolution of $m_{\rm SMS}$, obtained from solving coupled differential equations for $\dot{M}$, $\dot{R}_{\rm h}$, and $\dot{m}_{\rm SMS}$, where in the latter we use $m_{\rm SMS0} = 5\,{\rm M}_\odot$, $r_{\rm SMS0} = 6.7\,{\rm R}_\odot$, and $\delta = 0.5$ (see Section 2.3) and include both the gas accretion term ($\dot{m}_{\rm acc} = 5\,{\rm M}_\odot\,{\rm Myr}^{-1}$) and the contribution from stellar collision (equation 8). The models are solved until $t = \min(t_{\rm contr}, t_\infty)$. For the cluster with $N = 10^5$ (blue, dotted line) the runaway phase is interrupted because the relaxation driven expansion starts before the collision runaway formation of the SMS starts, i.e. $t_\infty \gtrsim t_{\rm contr}$. Note that because gas accretion is included in $\dot{m}_{\rm SMS}$, the critical N is slightly lower ($N \simeq 10^6$) than the estimate given in equation (11) ($N \simeq 1.4 \times 10^6$). The two larger clusters experience a runaway collision process before the contraction phase ends (i.e. $t_\infty < t_{\rm contr}$).

2.5 A capped collision rate

In the previous section we solved for $m_{\rm SMS}(t)$ by ignoring the feedback from binaries. This allows $m_{\rm SMS}$ to become as large as the mass of the cluster. As we will show here, a genuine runaway process will not happen because of dynamical feedback from binaries involving the SMS. At high stellar densities, stars can become bound to the SMS, either by triple interactions (Heggie 1975) or via tidal capture (Fabian, Pringle & Rees 1975). These binary systems are efficient in heating the surrounding stars in interactions, directly via accelerating stars and indirectly via ejecting stars (see e.g. Goodman 1984). As a result of the interactions the binary orbit shrinks, until the star collides with the SMS. A similar heating occurs when stars get captured by a massive central black hole inumericn the cluster core (Bahcall & Wolf 1976; Baumgardt, Makino & Ebisuzaki 2004a; Heggie et al. 2007). This is why the predicted exponential growth of the central star presented in the previous section (Fig. 1) will not occur: at some point the SMS-star binaries will generate enough energy to inflate the core, thereby decreasing the collision rate until some equilibrium is found (Heggie et al. 2007). We speculate that this is the reason why numerical simulations of stellar collisions in dense stellar cluster (Portegies Zwart & McMillan 2002; Portegies Zwart et al. 2004; Freitag et al. 2006; Mapelli 2016) always find that the second derivative of $m_{\rm SMS}(t)$ is negative, which is not expected in a runaway process.

The question is now: what sets the maximum collision rate? Heggie (1975) shows that the formation rate of hard binaries in three-body interactions scales as $m^3_{\rm SMS} n^2 / V^9_{\rm rms}$ (see also Chapter 22 of Heggie & Hut 2003 and Stodolkiewicz 1986), while the collision rate goes as $m^{1+\delta}_{\rm SMS} n / V_{\rm rms}$ (equation 8). We estimate the three-body binary formation rate at the hard–soft boundary from equation 1 of Stodolkiewicz (1986) for our typical initial conditions in Section 2.1 and for $m_{\rm SMS} = 100\,{\rm M}_\odot$. We can directly compare this binary formation rate to the collision rate following from equation (8). We find that the binary formation rate is roughly a factor of 2 larger. The stronger dependence on both $m_{\rm SMS}$ and the stellar number density in the binary formation rate means that this process becomes more important than direct collision as the SMS grows in mass and the cluster becomes denser. We assume that the SMS-star pairs form marginally bound and that the companion star collides with the SMS when the pericentre distance of its orbit equals $r_{\rm SMS}$. The specific orbital energy depends on the semimajor axis of the orbit, a, as $\epsilon_{\rm orb} \simeq -Gm_{\rm SMS}/(2a)$, where we assumed that $m_{\rm SMS}$ is much larger than the mass of the colliding star. For the colliding orbit, $a = r_{\rm SMS}/(1-\epsilon)$, where ϵ is the eccentricity of the orbit. We then find $\epsilon_{\rm orb} \simeq -Gm_{\rm SMS}(1-\epsilon)/(2r_{\rm SMS})$. A collision of a star with mass m is therefore accompanied by a dynamical energy supply of $\Delta E = m|\epsilon_{\rm orb}|$. Because the cluster dynamics becomes collisional near the moment of maximum stellar density (i.e. two-body effects become important), a natural assumption is that the rate at which dynamical energy is supplied to the cluster by binaries ($\dot{E}_{\rm bin}$) cannot exceed the flow of energy that can be transported through $R_{\rm h}$ by two-body relaxation, i.e.

$$\dot{E}_{\rm bin} \simeq \dot{m}_{\rm SMS}|\epsilon_{\rm orb}| \lesssim \zeta \frac{|E|}{\tau_{\rm rh}}, \tag{13}$$

where $E \simeq -GM^2/(4R_{\rm h})$ is the total energy of the cluster and $\zeta \simeq N^{-1}_{\rm rel} \simeq 0.1$ (Hénon 1961, 1965; Gieles, Heggie & Zhao 2011; Alexander & Gieles 2012). We then assume that all stars that collide with the SMS undergo this binary hardening phase in the collision phase, i.e. the collisions resulting from coalescence following binary formation and hardening are more efficient than direct stellar collisions, as the result of the decreased core density. We then find that the growth rate of the SMS is

$$\dot{m}^{\rm coll,\,rel}_{\rm SMS} = \zeta \frac{r_{\rm SMS}}{m_{\rm SMS}} \frac{M^2}{R_{\rm h}\tau_{\rm rh}}. \tag{14}$$

Here, we assumed that the orbital eccentricity is $\epsilon = 0.5$, and $\dot{m}^{\rm coll,\,rel}_{\rm SMS}$ would be higher for more eccentric orbits, and if stars start off more bound to the SMS (i.e. $\epsilon_{\rm orb} < 0$ when the binary forms). Comparing this with the expression for $\dot{m}^{\rm coll}_{\rm SMS}$ (equation 8), we see that this collision rate is less sensitive to the properties of the SMS, because it scales with $r_{\rm SMS}/m_{\rm SMS}$, as opposed to $r_{\rm SMS}m_{\rm SMS}$. This is because the collision rate is now set by how much energy can be transported by two-body relaxation, and the liberated energy is proportional to $m_{\rm SMS}/r_{\rm SMS}$.

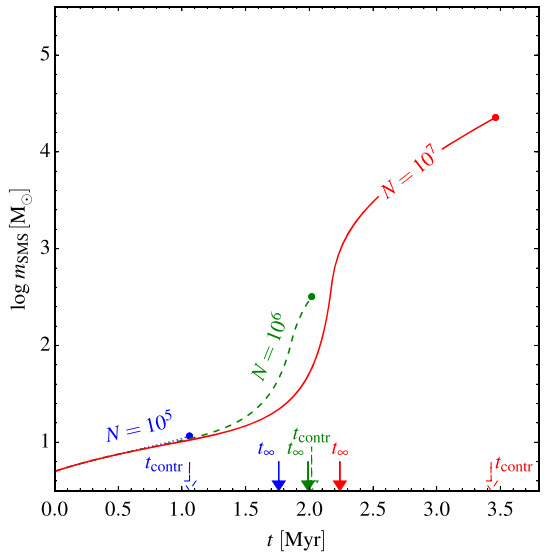

Figure 2. As Fig. 1, but now $\dot{m}^{\rm coll}_{\rm SMS}$ is limited by the flow of energy through the cluster (equation 14), which becomes relevant at $t \simeq t_\infty$. As before, the $N = 10^5$ cluster does not enter the runaway collision phase because $t_{\rm contr} < t_\infty$. For the larger N clusters, the collision rate is capped by two-body relaxation (equation 14) after ∼1 Myr ($N = 10^6$) and ∼1.5 Myr ($N = 10^7$).

Assuming that the cluster spends most of its time in this regime (i.e. $t_\infty << t_{\rm contr}$) and ignoring gas accretion on the SMS, we can derive $m_{\rm SMS}(t_{\rm contr})$ by integrating equation (14) from $t = 0$ to $t = t_{\rm contr}$ (i.e. similar to what Davis et al. 2010 did to estimate the total number of collisions in equal-mass clusters). Using the mass–radius relation for the SMS (equation 5), we then find

$$m_{\rm SMS}(t_{\rm contr}) \propto \left(\frac{r_{\rm SMS0} m_{\rm SMS0}^{5/6-\delta}}{\rho_{\rm h0}^{1/12}} N^{5/3} \dot{M}^{5/6} \right)^{1/(2-\delta)}. \quad (15)$$

If we again assume $\dot{M} \propto N$ then for fixed $m_{\rm SMS0}$, $r_{\rm SMS0}$, and $\rho_{\rm h0}$ we find

$$m_{\rm SMS}(t_{\rm contr}) \propto N^{5/(4-2\delta)} = \begin{cases} N^{5/4}, & \delta = 0, \\ N^{5/3}, & \delta = 1/2, \\ N^{5/2}, & \delta = 1. \end{cases} \quad (16)$$

For all reasonable assumptions for the uncertain mass–radius evolution of the SMS (i.e. the value of δ), the scaling $m_{\rm SMS}(N)$ is super-linear. Although we have not folded in mass-loss from the SMS, it is encouraging that massive GCs can form more SMS mass per unit cluster mass, which is required to explain the observed scalings of ΔY and $f_{\rm poll}$ with GC mass. In Fig. 2, we show the growth of $m_{\rm SMS}$ for a capped energy production rate, and otherwise the same conditions as in Fig. 1.

After collisions have become important, they are the dominant growth term. In our model, gas accretion on the SMS is proportional to its initial mass, but even if gas accretion is proportional to the instantaneous mass it would contribute an order of magnitude less to the growth of $m_{\rm SMS}$ than binary coalescence.

We now have a simple model for the formation of SMS via stellar collisions. We note that some aspects of this idea, such as the efficiency of cluster contraction following mass accretion and the collisional formation of SMSs, have already received some numerically validation (Davis et al. 2010; Moeckel & Clarke 2011). There are several uncertainties in the model presented in this section. First, the efficiency of the accretion of gas that flows into the cluster on to the protostars. We assumed this to be 100 per cent, but this needs to be verified with hydrodynamical simulations with high spatial and temporal resolution (e.g. Dale 2017; Gavagnin et al. 2017; Rey-Raposo et al. 2017; Smilgys & Bonnell 2017). Secondly, $r_{\rm SMS}$ is critical in the success of the enrichment model as we will discuss in the next section. Finally, the growth rate of $m_{\rm SMS}$ in the model relying on the capped collision rate depends on $\epsilon_{\rm orb}$ when the stars are captured, and the evolution of the eccentricity ϵ. Their values affect the constants of proportionality, and not the scaling with M and N. Other effects, such as the interaction of multiple companions of the SMS and the stellar mass function, which could potentially affect the scaling relations presented here, need to be understood as part of a detailed model for SMS growth. A numerical validation, similar to the work done on stellar disruption rates by an IMBH in GCs (e.g. Baumgardt, Makino & Ebisuzaki 2004a,b), would be an important future step. In the next section, we include the SMS formation model in a GC self-enrichment model.

3 AN EARLY SELF-ENRICHMENT MODEL

We use the SMS formation model of the previous section to develop a model for GC self-enrichment in the first few Myr of its formation. We start by putting together the different ingredients for GC and SMS formation and evolution in Sections 3.1 and 3.2. We add the effect of stellar winds in Section 3.3, which is required to pollute the intracluster medium with hot-hydrogen burning products of the SMS that end up in the chemical composition of the MSPs we observe today. We present the predictions for the evolution of the global properties of the SMS and their dependence with the total cluster mass in Section 3.4. We discuss all the other aspects of the early self-enrichment model in Section 4.

3.1 Cluster evolution

Cluster formation is complex because of the various physical processes at work on their respective time-scales, which makes a definition of when the cluster forms (i.e. $t = 0$) rather ambiguous. In our model, we define $t = 0$ as the start of the gas accretion phase, i.e. when the cloud has just fragmented. Magnetohydrodynamical models of star formation in turbulent clouds by Padoan, Haugbølle & Nordlund (2014, their fig. 13) show that protostars of any mass may take ∼1−2 Myr to form, with large variations in the assembly time-scale depending on the environment. Radiation hydrodynamics simulation of the collapse down to the protostar then show that this essentially proceeds on the free-fall time (Rosen et al. 2016), which is significantly shorter than 1 Myr for a clump massive enough to form a 100 M$_\odot$ star. For simplicity, we assume that the gas accretion phase dominates in the first 2 Myr, and that stars that are massive enough (typically ≥10 M$_\odot$) to go supernova reach zero-age main sequence at $t = 2$ Myr. This corresponds to the moment when the so-called stellar evolution phase starts (i.e. when H-burning ignites in the core of the stars more massive than 10 M$_\odot$; at that moment, low-mass protostars should still be on the Hayashi track, since typical PMS duration ranges between 10 and 100 Myr, see e.g. D'Antona & Mazzitelli 1994; Baraffe et al. 2002; Amard et al. 2016). We assume that gas accretion proceeds after this, although the efficiency may be reduced because of outflows (Federrath 2015; Offner & Chaban 2017). This timeline is illustrated in Fig. 3.

We solve for the change in cluster stellar mass as the result of gas accretion and mass-loss from stellar evolution as

$$\dot{M} = \dot{M}_{\rm acc} + \dot{M}_{\rm sev}, \quad (17)$$

where $\dot{M}_{\rm acc}$ describes the gas accretion and is given by

$$\dot{M}_{\rm acc} = \begin{cases} \langle \dot{m}_{\rm acc} \rangle \, N & t < 5\,{\rm Myr} \\ 0 & t \geq 5\,{\rm Myr}, \end{cases} \quad (18)$$

with $\langle \dot{m}_{\rm acc} \rangle = 0.1\,{\rm M}_\odot\,{\rm Myr}^{-1}$. We assume that at $t > 5$ Myr the gas accretion is halted by stellar feedback. This time corresponds to the moment when massive stars have an age of 3 Myr, i.e. close to the typical theoretical lifetime of a $120\,{\rm M}_\odot$ star (∼3.5 Myr, see e.g. Georgy et al. 2013). After $t = 5$ Myr, the stellar mass decreases as the result of stellar mass-loss. In the first 10 Myr of massive star evolution (typical theoretical lifetime of a $15\,{\rm M}_\odot$ star, Georgy et al. 2013), a stellar population loses about 10 per cent of its mass, so we use

$$\dot{M}_{\rm sev} = \begin{cases} 0 & t < 5\,{\rm Myr} \\ -0.1\,M/t & t \geq 5\,{\rm Myr}. \end{cases} \quad (19)$$

Note that in equation (17) we do not subtract the mass of stars that end up on the SMS, because this (negative) contribution is negligible in most models. The half-mass radius of the cluster evolves as

$$\dot{R}_{\rm h}(N, M, R_{\rm h}) = -3\frac{\dot{M}}{M}R_{\rm h} + \zeta\frac{R_{\rm h}}{\tau_{\rm rh}}, \quad (20)$$

where the first contribution is due to the mass evolution and the second contribution describes the expansion due to two-body relaxation. Before $t = 5$ Myr, the first term describes the adiabatic contraction ($\dot{M} > 0$, $\dot{R}_{\rm h} < 0$) described in Section 2.2, and after $t = 5$ Myr it describes the expansion ($\dot{M} < 0$, $\dot{R}_{\rm h} > 0$) following stellar evolution mass-loss. For homologous and adiabatic mass-loss, the cluster expands as $\dot{R}_{\rm h}/R_{\rm h} = -\dot{M}/M$ (Hills 1980), but because most of the stellar mass-loss occurs in the centre where the massive stars reside, the factor of 3 approximates the enhanced expansion as the result of mass segregation. We use equation (2) for $\tau_{\rm rh}$, with the parameters described in Section 2.2. As long as $\tau_{\dot{M}} << \tau_{\rm rh}$ in the first 5 Myr, the first term dominates and the cluster contracts, until $\tau_{\dot{M}} \simeq \tau_{\rm rh}/\zeta$, after which relaxation starts to dominate the evolution and the cluster expands as the result of two-body heating by SMS-star binaries. For clusters without gas accretion, this relaxation driven expansion results in a radius evolution of the form $R_{\rm h} \propto t^{2/3}$ (Hénon 1961), but in our case the radius expands more slowly because of the gas accretion, which contributes negatively to $\dot{R}_{\rm h}$.

With the evolution of M and $R_{\rm h}$ of the cluster, we can now consider the evolution of the SMS in its centre.

3.2 Hypothesis for the mass growth of the SMS (gas accretion and collisions)

The SMS mass grows as the result of gas accretion and stellar collisions. Its rate of growth as a function of the cluster properties and its own properties is given by

$$\dot{m}_{\rm SMS} = \dot{m}_{\rm acc} + \min\left(\dot{m}^{\rm coll}_{\rm SMS}, \dot{m}^{\rm coll,\,rel}_{\rm SMS}\right). \quad (21)$$

Here, $\dot{m}_{\rm acc}$ is the rate of growth as the result of gas accretion, and as discussed in Section 2.2, we adopt an accretion rate that is proportional to the stellar mass at the time of fragmentation, i.e. $\dot{m}_{\rm acc} = m_{\rm SMS0}\,{\rm Myr}^{-1}$, and we adopt an initial mass and radius of the SMS of $m_{\rm SMS0} = 5\,{\rm M}_\odot$ and $r_{\rm SMS0} = 6.7\,{\rm R}_\odot$ (see Section 2.3). The exact value of $m_{\rm SMS0}$ is not very important, because the onset of the runaway collision process (i.e. t_∞) is very insensitive to $m_{\rm SMS0}$ and $r_{\rm SMS0}$ (see equation 10). The second term contains the two mass growth rates due to collisions discussed in Section 2: $\dot{m}^{\rm coll}_{\rm SMS}$ is given by equation (8) and describes the growth of the SMS before it is regulated (i.e. capped) by relaxation, which becomes important when $\dot{m}^{\rm coll,\,rel}_{\rm SMS} < \dot{m}^{\rm coll}_{\rm SMS}$ and then the SMS grows at a rate $\dot{m}^{\rm coll,\,rel}_{\rm SMS}$, given by equation (14).

The radius of the SMS is passively evolved via the mass–radius relation of equation (5) and we adopt values of $\delta = 0.5$ and $\delta = 1$.

3.3 Hypothesis for the mass-loss of the SMS by stellar winds

Hot massive stars experience a strong mass-loss by stellar winds. We will estimate the radiation driven mass-loss rates for very massive stars and SMSs based on the stellar models of SMSs with $m_{\rm SMS} > 100\,{\rm M}_\odot$ from Nadyozhin & Razinkova (2005). Very massive main-sequence stars are largely convective, due to their high luminosity. This implies that their dimensionless structure is (almost) independent of the energy source, which facilitates the calculation of the mass–luminosity relation. The main parameter that determines the structure and luminosity of the star is $\mu^2 m_{\rm SMS}$, where μ is the mean particle mass ($\mu = 0.60$ for $X = 0.75$, $Y = 0.25$, $Z = 0.001$).

The total potential plus kinetic energy of a radiation driven wind cannot exceed the stellar luminosity. This implies that $0.5\dot{m}_{\rm wind}(v^2_{\rm esc,\,SMS} + v^2_\infty) < l_{\rm SMS}$ or $\dot{m}_{\rm wind} < l_{\rm SMS} r_{\rm SMS}/(G m_{\rm SMS})$. Here, $v_{\rm esc,\,SMS}$ is the escape velocity from the surface of the SMS and v_∞ is the terminal wind velocity. This is a severe upper limit, because it implies that the total luminosity is used to drive the wind and no light will leave the star. A more realistic estimate is obtained if we assume that the total momentum of all the photons is used to drive the wind. This results in $\max(\dot{m}_{\rm wind}) = l_{\rm SMS}/(c v_\infty)$. Multiple scattering of photons, as occurs e.g. in the winds of Wolf–Rayet stars, can increase this upper limit by at most a factor $f \simeq 3$ (Vink et al. 2011). Terminal wind velocities of radiation driven winds scale with $v_{\rm esc,\,SMS}$, i.e. $v_\infty = a v_{\rm esc,\,SMS}$, with $a = 2.6$ for stars with $T_{\rm eff} > 20\,{\rm kK}$ and $a = 1.3$ for stars with $10 < T_{\rm eff}/{\rm kK} < 20$ (Lamers & Cassinelli 1999). This results in an estimate of

$$\max(\dot{m}_{\rm wind}) = \frac{f}{a}\frac{l_{\rm SMS}}{c}\sqrt{\frac{r_{\rm SMS}}{2Gm_{\rm SMS}(1-\Gamma)}}, \simeq 10^{-4}\,{\rm M}_\odot\,{\rm yr}^{-1}\left(\frac{m_{\rm SMS}}{100\,{\rm M}_\odot}\right)^{1/2+\delta/2}. \quad (22)$$

The maximum mass-loss rates derived here agree with the mass-loss rates calculated by Vink et al. (2011) for very massive stars (so called $\gtrsim$100 $\rm M_\odot$) with solar metallicity. However, Vink, de Koter & Lamers (2001) and Vink (2018) have shown that the mass-loss rates depend on metallicity as $\dot{m}_{\rm wind} \propto Z^{0.8}$. If this also holds for SMSs, the mass-loss rates of low metallicity ZAMS stars with $Z = 0.001$ may be 10 times smaller.

The estimates described above are for H-rich main-sequence stars. As the stars evolve almost homogeneously, because they are largely convective, the H-abundance decreases and the He-abundance increases. As the He-abundance increases, μ increases and the opacity $\sigma_{\rm e}$ decreases due to the reduced abundance of electrons. This results in an increase in luminosity and an increase in the Eddington luminosity, because $l_{\rm Edd} \propto m_{\rm SMS}/\sigma_{\rm e}$. Vink et al. (2011) have shown that the mass-loss rate increases strongly with the ratio $\Gamma = l_{\rm SMS}/l_{\rm Edd}$ for stars close to their Eddington limit. In fully convective stars, Γ increases as a function of $\mu^2 m_{\rm SMS}/\sigma_{\rm e}$ (Nadyozhin & Razinkova 2005). Both factors $m_{\rm SMS}$ and $\mu^2/\sigma_{\rm e}$ increase during the build-up of a SMS, so the luminosity approaches the Eddington limit and the mass-loss rate will increase.

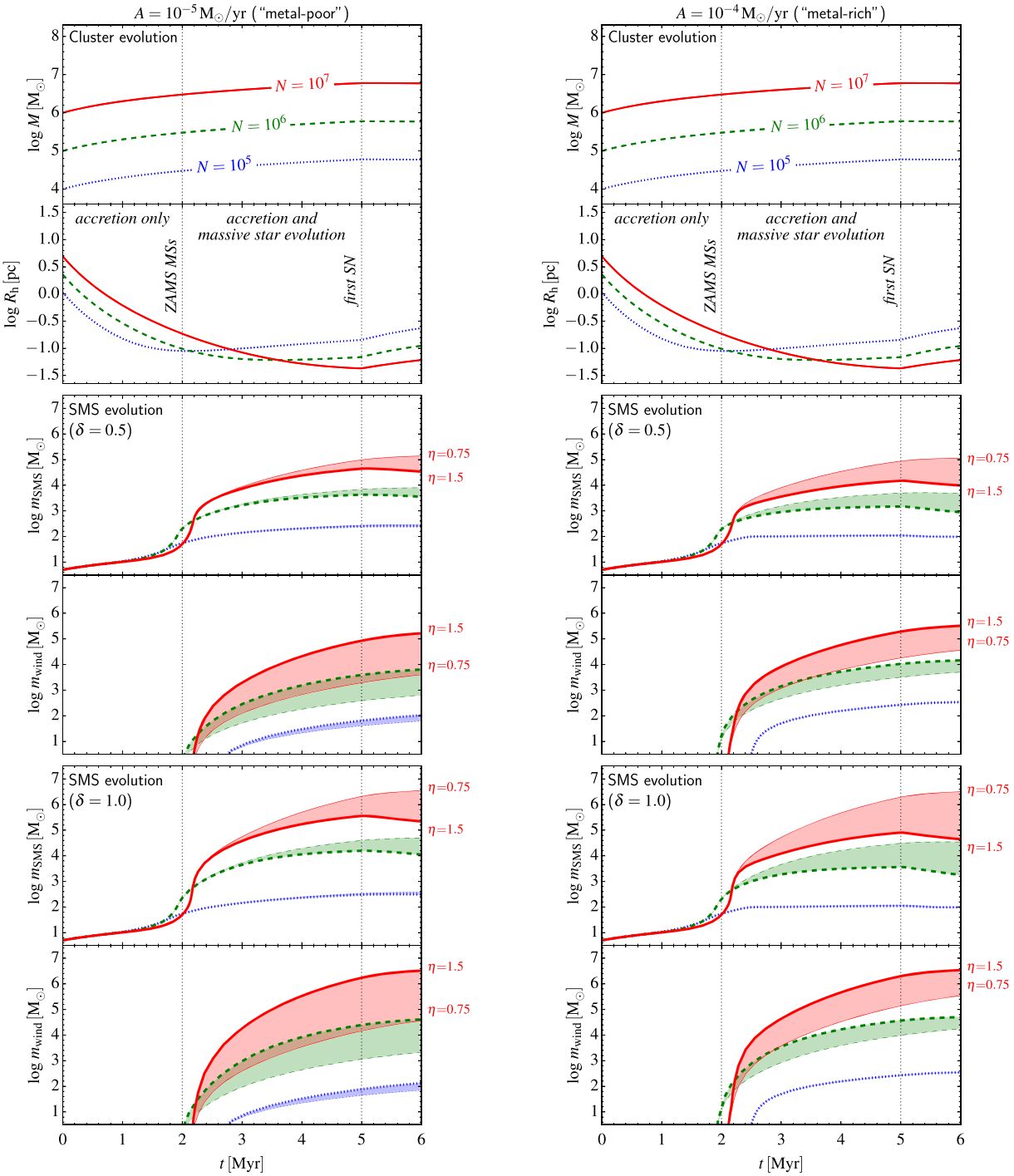

Figure 3. Model for SMS formation in a GC that accretes gas until $t = 5$ Myr. As stated in Section 3.1, gas accretion and cluster contraction starts at $t = 0$ and the first massive stars $>10\,M_\odot$ reach the ZAMS at $t = 2$ Myr. The possible occurrence of the first SNe (from stars of $\sim$120 $M_\odot$, main-sequence lifetime $\sim$3 Myr) is also indicated. Left-hand panels show the results for the metal-poor clusters/SMSs with the lower $\dot{m}_{\rm wind}$ ($A = 10^{-5}\,M_\odot\,{\rm yr}^{-1}$ in equation 23), and the right-hand panels show the result for the metal-rich case ($A = 10^{-4}\,M_\odot\,{\rm yr}^{-1}$). The cluster M and $R_{\rm h}$ evolve according to equations (17) and (20), respectively. The SMS mass and radius are evolved using equations (21) and (5), respectively, for $\delta = 0.5$ (middle panels) and $\delta = 1$ (bottom panels). The thick lines show the result for $\eta = 0.75$ in equation (23) and the thin lines show the results for $\eta = 1.5$. The middle panels show the accumulated mass liberated by the SMS in winds (from equation 23) for $\delta = 0.5$, while the bottom two panels show the result for $\delta = 1$. For stronger winds ($\eta = 1.5$), $m_{\rm SMS}$ grows more slowly, but more mass is liberated.

These estimates refer to stars in thermal and dynamical equilibrium. However, as a SMS accretes a massive star, it may be out of equilibrium during a fraction of the Kelvin–Helmholtz time-scale that is about 10^4 yr for a 300 $M_\odot$ star at the main sequence and 10^3 yr for a He star. At that time the $T_{\rm eff}$ may be considerably lower than the value adopted above (Glebbeek et al. 2009). We can obtain an estimate of $T_{\rm eff}$ from the study of LBVs, which increase their radius and decrease their $T_{\rm eff}$ during outbursts to about 10 kK

(Humphreys & Davidson 1994). Substituting this low value of $T_{\rm eff}$ in the formalism described above, and adopting the corresponding value of $a = 1.3$, we find a maximum radiation driven mass-loss rate that is a factor five larger than predicted by equation (22). This results in a mass-loss rate of $3 \times 10^{-4}\,{\rm M}_\odot\,{\rm yr}^{-1}$ for an LBV of $60\,{\rm M}_\odot$, which is close to the observed mass-loss rates of LBVs during outburst. If a SMS captures stars at a rate of order one per 10^4 yr or faster, the star will be out of equilibrium for most of its lifetime, so the time-averaged mass-loss rate will be higher than for stars in equilibrium and may resemble that of LBVs. Given these arguments, we adopt a simple relation

$$\dot{m}_{\rm wind} = A \left(\frac{m_{\rm SMS}}{100\,{\rm M}_\odot} \right)^{\eta}, \qquad (23)$$

with $A = 10^{-4}\,{\rm M}_\odot\,{\rm yr}^{-1}$ and $10^{-5}\,{\rm M}_\odot\,{\rm yr}^{-1}$ to allow for the possible mass-loss reduction of SMS of low metallicity, and $\eta = 0.75$, corresponding to constant $T_{\rm eff}$ (i.e. $\delta = 1/2$), and $\eta = 1.5$ to account for the increasing mass-loss rate as the He content increases.

3.4 Predicted evolution of the SMS global properties, and dependence on the cluster mass

With all the ingredients of the previous sections in place, we are now able to solve for the evolution of M and $R_{\rm h}$ and the SMS properties $m_{\rm SMS}$ and $r_{\rm SMS}$. We solve the coupled ordinary differential equations of the previous sections with the 'dopri5' integrator (Hairer, Nørsett & Wanner 1993), which is a Runge–Kutta integrator with adaptive step-size to calculate fourth and fifth order accurate solutions. It is supplied by the SCIPY sub-package INTEGRATE. The mass that is lost from the SMS by winds ($m_{\rm wind}$) is the amount of polluted material that is available for recycling into MSPs.

The most uncertain parameters are δ in the SMS mass–radius relation (equation 5) and A and η, which set the strength of the stellar wind as a function of $m_{\rm SMS}$ (equation 23). We therefore vary all three. Fig. 3 shows the result of the model for $\delta = 0.5$ and $\delta = 1$ for a relatively low $\dot{m}_{\rm wind}$ ($A = 10^{-5}\,{\rm M}_\odot\,{\rm yr}^{-1}$), corresponding to the metal-poor conditions (left-hand panels) and for a relatively high $\dot{m}_{\rm wind}$ ($A = 10^{-4}\,{\rm M}_\odot\,{\rm yr}^{-1}$), corresponding to the metal-rich regions (right-hand panels). The two top panels show the evolution of cluster M and $R_{\rm h}$ for clusters with different N. The middle panels show $m_{\rm SMS}$ and $m_{\rm wind}$ for $\delta = 0.5$, where the thick lines show the result of $\eta = 0.75$ (i.e. $\dot{m}_{\rm wind} \propto m_{\rm SMS}^{0.75}$) and the thin lines are for $\eta = 1.5$. For larger $\dot{m}_{\rm wind}$ (higher η), the SMS reaches lower masses, but releases more mass in winds. The bottom panels of Fig. 3 shows similar results, but for $\delta = 1$.

The small difference in δ has a large effect on $m_{\rm SMS}$ and $m_{\rm wind}$. Because for larger δ the SMS has a larger $r_{\rm SMS}$, it has a larger cross-section making collisions more frequent in the early phases. At later stages, the effect of a larger $r_{\rm SMS}$ is that the collisions result in a lower energy production, because the colliding stars feel less of the gravitational potential of the SMS when they collide. The most massive cluster ($N = 10^7$) forms a SMS reaching a mass of $\sim$10 per cent of the cluster mass, whereas $m_{\rm wind}$ can be an order of magnitude larger than max ($m_{\rm SMS}$), because of continuous rejuvenation of the SMS via collisions. We notice that for $\delta = 1$, the total mass of processed material, $m_{\rm proc} = m_{\rm SMS} + m_{\rm wind}$, is insensitive to A and η. For $N = [10^5, 10^6, 10^7]$, we find $m_{\rm proc}/{\rm M}_\odot \simeq [870, 39\,000, 1\,629\,000]$, or $m_{\rm proc}/M \simeq [0.015, 0.057, 0.37]$. For $\delta = 0.5$, models with an order of magnitude larger A result in 10 per cent larger $m_{\rm proc}$ (for a given N), and varying η from 0.75 to 1.5 results in a maximum increase of $m_{\rm proc}$ by a factor of 2. In conclusion, $m_{\rm proc}$ is most sensitive to N and δ. This 'conveyor belt' production of material processed through the SMS 'nuclear reactor' allows this SMS scenario to overcome the mass budget problem discussed in Section 1.

Because the SMS wind is released while the cluster is still accreting (cold) gas, the wind material can remain in the cluster: the hot, processed material from the SMS wind mixes with the cold pristine gas, which subsequently accretes on the protostars (see Section 4.1 for more details). The bottom panels of Fig. 3 show that sufficient material can be produced in a few Myr to account for the observed proportions of chemically anomalous low-mass stars in GCs (we discuss this further in Sections 4.2 and 4.3). A schematic representation of the GC enrichment scenario is shown in Fig. 4. In the next section, we discuss several aspects of this GC self-enrichment scenario in more detail.

4 DISCUSSION

In this section, we discuss several aspects and uncertainties of the model presented in Section 3 in more detail and we make observational predictions.

4.1 Mixing of SMS wind and pristine gas

Ejecta in stellar winds in general and likely also in winds from SMSs have high velocities, typically of the order of a $10^3\,{\rm km\,s}^{-1}$ (e.g. Muijres et al. 2012; also for our SMS model of Section 2.3 we find $v_\infty \simeq 3000\,{\rm km\,s}^{-1}(m_{\rm SMS}/100\,{\rm M}_\odot)^{1/2-\delta/2}$). This may exceed the escape velocity of our modelled star clusters. For a King (1966) model with dimensionless central potential $W_0 = 9(10)$, we find that the escape velocity from the centre of the cluster is[6] $V_{\rm esc}(0) \simeq 490(545)\,{\rm km\,s}^{-1}\sqrt{M/10^6\,{\rm M}_\odot}\sqrt{0.1\,{\rm pc}/R_{\rm h}}$. The SMS is assumed to be in the very centre, because this is where the collision rate is highest and if it is displaced by collisions, it rapidly sinks back via dynamical friction. Interaction with ambient gas slows down the ejecta so they can accrete on the low-mass protostars. Interestingly, we do not expect the stellar winds, including the SMS wind to push out the dense gas from the cluster in the case of massive, compact star clusters, as investigated in the present study (Krause et al. 2016): for a Salpeter mass function, stellar winds cannot remove the gas if $V_{\rm rms}$ exceeds a critical value that is in the range[7] 10–30 $\,{\rm km\,s}^{-1}$, depending on the star formation efficiency. This is still applicable for our modelled clusters that contain SMSs, because the mass-loss rate of the SMS is comparable to or less than the combined mass-loss rate of the other massive stars.

For our lowest mass cluster with $N = 10^5$, i.e. initially $10^4\,{\rm M}_\odot$ in stars, $V_{\rm rms}$ stays between 8 and $15\,{\rm km\,s}^{-1}$ (derived from Fig. 3). So as star formation proceeds, we expect some gas to be removed. The higher mass clusters have $V_{\rm rms} > 30\,{\rm km\,s}^{-1}$ throughout and will therefore not lose gas due to the stellar winds.

Can the ejecta mix with pristine gas? This should not simply be assumed, as for example in the Milky Way, observations of radioactive massive star ejecta show that there is no mixing for at least $\sim$1 Myr after ejection (Kretschmer et al. 2013; Krause et al. 2015). The SMS wind is, however, efficiently caught in such a star cluster. To see this, we first calculate the stall radius of the SMS wind where the bulk velocity of the wind $v_\infty = v_3\,10^3\,{\rm km\,s}^{-1}$ is thermalized at

[6] We use the LIMEPY models (Gieles & Zocchi 2015) to compute $V_{\rm esc}(0)$.
[7] Note that Krause et al. (2016) use a compactness parameter $C_5 = (M/10^5{\rm M}_\odot)(R_{\rm h}/{\rm pc})^{-1} \propto V_{\rm rms}^2$.

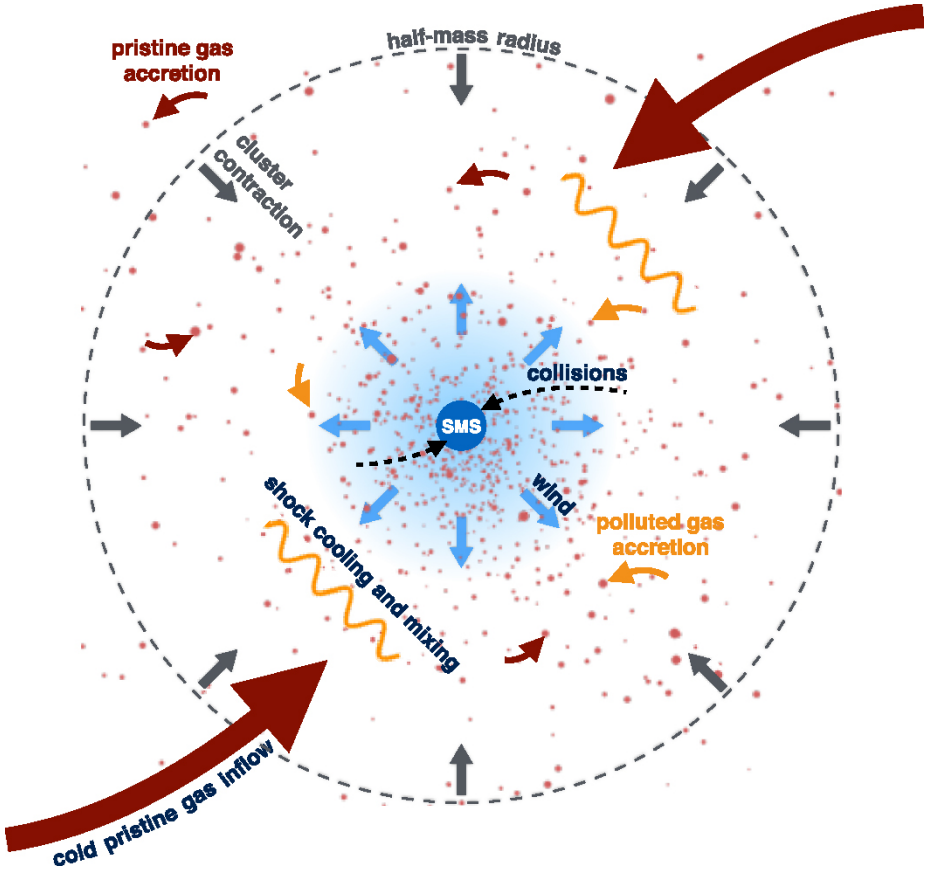

Figure 4. Schematic picture of the enrichment scenario presented in Section 3. Cold, pristine gas accretes on to the stars in the cluster, causing the cluster to contract. The higher stellar density results in stellar collisions, forming a SMS in the cluster centre. The SMS blows a wind enriched in hot-hydrogen products, which interacts and mixes with the inflowing gas. The mixed material subsequently accretes on to the stars enriching them with SMS yields.

the inner shock. The stall radius, $R_{\rm stall}$, is defined by the ram pressure, which declines with distance r from the SMS as r^{-2}, matching the ambient pressure P. The general pressure level is set by the gravitational potential, $P = fGM^2/R_{\rm h}^4$, where $M = 10^6 M_6\,{\rm M}_\odot$ is the total mass of the system and $f \lesssim 1$ is a function of the detailed mass distribution. Ram pressure balance, $\rho v_\infty^2 = P$, then implies

$$R_{\rm stall} = 10^{-5}\,{\rm pc}\,|\dot{M}_2|^{1/2} v_3^{1/2} R_{\rm h,-1}^2 f^{-1/2} M_6^{-1}, \quad (24)$$

where $R_{\rm h} = 0.1 R_{\rm h,-1}$ pc and $\dot{M} = 10^2\,\dot{M}_2\,{\rm M}_\odot\,{\rm Myr}^{-1}$. This is very small compared to the size of our cluster for all reasonable choices of parameters. The SMS wind density at the stall radius is given by

$$\rho = 10^{-15}{\rm g\,cm^{-3}}\, v_3^{-2} M_6^2 R_{\rm h,-1}^{-4}. \quad (25)$$

This is so high that the ejecta, which will first be heated to keV temperatures at the wind shock, will cool down instantly via emission of bremsstrahlung and collisionally excited line emission, and clump via the thermal instability. The resulting cold gas will integrate naturally into the ongoing accretion flows on to the low-mass stars/clumps. The recent proposal by Szécsi, Mackey & Langer (2018) that polluted stars might be formed in the photoionized shells of very massive supergiants is conceptually similar, also relying on high gas densities. Low-mass stars observed with extreme (low) oxygen abundances formed out of essentially pure hot hydrogen burning ejecta, i.e. with a dilution factor with pristine material less than 10–30 per cent (respective values for NGC 2808 and NGC 6752, see Prantzos et al. 2017). Complete mixing before accretion from the intracluster medium can therefore not take place (details in Section 4.2). Instead, we have to postulate that extreme stars form close to the stall radius where the intracluster medium should predominantly consist of SMS ejecta. Details are complex and are beyond the scope of this work. Importantly, the inability of the system to lose dense gas via stellar feedback (compare above) will ensure that all the cold gas, including the cooled-down ejecta will end up in low-mass stars.

4.2 Nucleosynthesis in SMSs, composition of their ejecta, and dilution with pristine gas

The key points of the 'conveyor belt' mechanism for the production of the observed abundance anticorrelations and the moderate enrichment of He by a SMS are the following: (1) a SMS is a fully convective object, with a convection flow time-scale ($\tau_{\rm conv} \leq$ yr) many orders of magnitudes shorter than the time-scale for nuclear fusion; (2) the nuclear reactions that produce the anticorrelations reach an equilibrium on a time-scale much shorter ($\tau_{\rm NaO} \sim$ yr) than the main-sequence lifetime for the full conversion of H into He ($\tau_{\rm He} \sim 0.2-2$ Myr, depending on the SMS mass); (3) the products of nuclear fusion are spread throughout the star by convection so that a large fraction of the SMS is quickly enriched and partly ejected in the wind; (4) collisions constantly refurnish the stellar interior with low He content material on an intermediate time-scale ($\tau_{\dot{m}_{\rm SMS}} \sim 0.1$ Myr). The relative time-scales, i.e. $\tau_{\rm conv} \lesssim \tau_{\rm NaO} \ll \tau_{\dot{m}_{\rm SMS}} < \tau_{\rm He}$, ensures the efficient production and

release of CNONaMgAl processed material, whilst keeping low the He abundance inside the SMS and its wind.

Consequently, we can discuss nucleosynthesis in SMSs by focusing on their central temperature and assume that the material they eject at a given evolution time has the same chemical composition as the central regions where hot H-burning occurs, with the difference that He remains relatively constant. Here, we base our discussion on SMS models presented in Denissenkov et al. (2015) and in Prantzos et al. (2017) as well as additional models for the metallicity range relevant for GCs computed by P. Denissenkov with the same stellar evolution code MESA (Paxton et al. 2011, 2013) and the same input physics (Denissenkov, private communication). These models cover the mass range between 10^3 and 7×10^4 $M_\odot$, and $-2.2 < [Fe/H] < -0.5$. Accretion and rotation are not accounted for in the computations; we assume that this does not affect the nucleosynthesis picture, nor the time-scales.

Over the whole mass and metallicity range considered, SMS models reach high enough central temperature ($\geq$60 MK) to run CNO and NeNa at equilibrium already at the very beginning of the main sequence (see fig. 4 of Prantzos et al. 2017, for models with $[Fe/H] = -1.5$). Therefore, in all SMS models the C–N and O–Na anticorrelations build up immediately for very low He enrichment ($\Delta Y < 0.01$, in agreement with the observationally inferred variation in the He content of most GCs). However, a minimum SMS mass of $\sim 5 \times 10^3$ $M_\odot$ is required to reach the Mg-burning temperature ($\sim$75−80 MK) early on the main sequence with similarly low He enrichment (fig. 4 of Prantzos et al. 2017). Because of the relation between the mass and the central temperature of the stars, we thus expect the Mg–Al anticorrelation to be present only in the most massive clusters where the more massive SMS can form (see Section 3.4).

A metallicity dependence is also expected, as stars of a given mass reach hotter temperature on the early main sequence when metallicity decreases. Additionally, $\dot{m}_{\rm wind}$ is lower at low metallicity, leading to larger $m_{\rm SMS}$. Thus for a given cluster mass, more extreme Mg-depletion is foreseen at lower metallicity. This nicely explains the finding of a bivariate relation of the Mg spread as a function of M and [Fe/H] in Galactic GCs (Carretta et al. 2009b; Pancino et al. 2017).

In the current SMS models, which are computed without accretion nor rejuvenation by stellar collisions, the central temperature strongly increases at the end of the main sequence, up to values where Na and Al efficiently burn through p-captures. This is predicted to occur for $\Delta Y \gtrsim 0.55$ (see fig. 4 of Prantzos et al. 2017), i.e. for He enrichment more extreme than allowed by the current photometric constraints (ΔY between 0.01 and 0.18, see references in Prantzos et al. 2017). Therefore, SMSs are in principle successful to get the right chemistry to explain the whole observed abundance patterns, but only in their early main-sequence nuclear burning configuration. In the 'conveyor belt' scheme we actually expect SMS to reach an equilibrium state that allows them to stay in these conditions as collisions constantly bring fresh material with low He content that is instantaneously mixed within the convective interior of the SMS. Varying dilution factors between SMS ejecta with low He content and material with pristine composition nicely accounts for the whole range of abundances observed along the anticorrelations (e.g. fig. 1 in Denissenkov et al. 2015 and fig. 7 in Bastian et al. 2015). These variations should be directly related to the varying amounts of SMS ejecta that are accreted by individual low-mass protostars. In particular, one can speculate that the clumps located in the more central regions closer to the SMS form the stars with the most extreme abundance variations, while those in the more external regions of the cluster form stars with chemical composition closer to the original one. This accounts for the fact that polluted stars are generally more concentrated in the innermost region than pristine stars (e.g. Lardo et al. 2011; Simioni et al. 2016), although there are clusters, such as M15, for which the relative radial distribution may be reversed in the very inner parts (Larsen et al. 2015, but see Nardiello et al. 2018). Because of the short relaxation time-scale in the centre, the radial distribution of stars in the core is actually unlikely to be the result of the initial conditions. Similarly, the relative amounts of pristine and processed gas present in the cluster should be a function of time, with more pristine gas being available in the beginning. This should also contribute to the spread in the abundance pattern (Decressin, Charbonnel & Meynet 2007b). Estimates of the total dilution factor using different constraints (e.g. the extent and shape of the O–Na and Li–Na anticorrelations) indicate that the overall process operated approximately in the 1:1 dilution regime (Prantzos et al. 2017). In the next section, we discuss several elemental abundances in more detail.

4.3 Abundances of various elements

4.3.1 Sodium

Fig. 6 of Carretta et al. (2009a) shows the Na–O anticorrelation for about 2000 stars in 19 different GCs. From this we see that a typical GC star has a Na abundance that is about 2.5 times higher than that of pristine stars in the Milky Way halo. Considering that the material in the stars is the result of material with pristine abundance $X_{\rm pristine}$ and processed material with abundance $X_{\rm processed}$, then the resulting abundance of the mixed material $X_{\rm mixed}$ can be written as

$$X_{\rm mixed} = \frac{X_{\rm processed} + f X_{\rm pristine}}{1 + f}, \quad (26)$$

where f is the dilution factor, i.e. one part of processed material is mixed with f parts of pristine material (e.g. Prantzos et al. 2017), which in our model can be written as $f = M/m_{\rm wind} - 1$. For $X_{\rm mixed}/X_{\rm pristine} = 2.5$, as estimated from the Carretta et al. results, we find $f = (X_{\rm processed}/X_{\rm pristine} - 2.5)/1.5$, or $f \simeq 5$ for $X_{\rm processed}/X_{\rm pristine} \simeq 10$ (see fig. 1 in Denissenkov et al. 2015). Using the bottom panels of Fig. 3, we see the required $M/m_{\rm wind} = 6$ (i.e. $f = 5$) is feasible. For $\eta = 1.5$, we find $M/m_{\rm wind} \simeq 10(2)$ for $N = 10^6(10^7)$ (almost independently of A). From this we see that it is in principle possible to produce sufficient amounts of Na in this SMS scenario. We note that the dilution tracks of SMS yields reproduce the shape of the O–Na anticorrelation (Denissenkov & Hartwick 2014). As explained in Prantzos et al. (2007, 2017), O is at equilibrium at the temperature where Na is produced, and the minimum dilution factor along the O–Na anticorrelation is actually set by the observed extreme O abundances. Therefore, reproducing the Na enrichment implies that we also get the correct amount of O depletion.

4.3.2 Helium

Piotto et al. (2007) estimate the amount of additional He that is needed to explain the two main sequences bluewards of the pristine main sequence in NGC 2808, one of the clusters displaying some of the most extreme multiple population features (see also Milone et al. 2015). One of the populations needs 2.2×10^4 $M_\odot$ additional He and the second one needs 9.1×10^3 $M_\odot$ additional He. For a mass fraction of $Y \simeq 0.4$ this implies a total mass of SMS processed material of $m_{\rm wind} \simeq (2.2 + 0.9)/0.6 \simeq 5 \times 10^4$ $M_\odot$. This assumes that the SMS ejecta have $Y = 0.4$ independent of time, which is of

course oversimplified. However, in Section 3.3 we discussed that $\dot{m}_{\rm wind}$ goes up quickly if the He abundance increases and $m_{\rm SMS}$ increases, hence most material will be ejected in the later stages of the SMS evolution. From Fig. 3, we see that this is achievable even with less favourable choice of $\eta = 0.75$ and $\delta = 0.5$ for $N = 10^7$. Milone et al. (2014) shows ΔY as a function of M_V and finds that a typical cluster with $M_V \simeq -7.5$ has $\Delta Y \simeq 0.03$. If we again assume that the processed material has Y= 0.4, then for a present-day GC mass of $2 \times 10^5\,{\rm M}_\odot$ we (only) need $1500\,{\rm M}_\odot$ in He, or $m_{\rm wind} \simeq 2500\,{\rm M}_\odot$. From Fig. 3, we see that this is also achievable for lower mass GCs with $N = 10^6$. Because the exact He abundance of the wind is very uncertain, because of the sensitive dependence on various time-scales, it is difficult to make strong predictions at this point. However, from the rough estimates here we conclude that it is possible for a single SMS to produce sufficient amount of He, even for the most extreme (i.e. the most massive) clusters.

4.3.3 Lithium

In our model, H-processed material from the SMS wind mixes with inflowing pristine material. Because the CNONaMgAl abundance patterns are produced at high temperatures, all the fragile Li (burning temperature of ∼2.5 MK) is destroyed inside the SMS and the wind material is Li free. However, thanks to dilution of SMS ejecta with pristine material (Section 4.2), it is expected that right after cluster formation there is a Li–Na anticorrelation in the material that can be accreted by the newly forming protostars (e.g. Lind et al. 2011). In this framework, the maximum initial Li abundance in a given star at birth obviously depends on the Li content of the pristine gas, on the amount of dilution with SMS ejecta, and on the moment when polluted material is accreted by the newly forming star (very fast accretion is actually needed to maintain a non-negligible lithium content in the accreting star; D'Antona et al. 2014, Salaris & Cassisi 2014).

Importantly, the photospheric Li abundance of GC low-mass stars is expected to decrease as a result of the combination of several processes at act in their interiors along their evolution. This includes nuclear burning in the fully convective phase and thermohaline mixing induced by accretion once a radiative core has developed on the pre-main sequence, atomic diffusion in the presence of weak turbulence, mass-loss, rotation-induced mixing, and internal gravity waves along the main sequence, and dredge-up and thermohaline mixing along the red giant branch (for references see e.g. Pinsonneault, Charbonnel & Deliyannis 2000 and Charbonnel 2016). These processes are known to modify the surface Li abundance of Population I main-sequence and giant stars (including the Sun and field and open cluster stars). They could thus potentially explain why the primordial Li abundance, as derived from *Planck* (Cyburt et al. 2016) is about three times larger than what is found in Pop II stars in the Milky Way (e.g. Spite & Spite 1982; Charbonnel & Primas 2005; Meléndez et al. 2010; Sbordone et al. 2010) and its GCs (Charbonnel 2006; Korn et al. 2006, 2007; Monaco et al. 2010; Mucciarelli et al. 2011; Gruyters et al. 2016). These processes could also blur the initial Li–Na anticorrelation, through differential effects all along the evolution of GC stars born with different initial masses, chemical compositions, and rotation rates.

As a matter of fact, observational hints for a Li–Na anticorrelation were found in old GCs, but only in the case of studies focusing on main-sequence turnoff stars (Pasquini et al. 2005; Bonifacio et al. 2007; Lind et al. 2009). We argue that the absence of a Li–Na anticorrelation in studies focusing on red giant GC stars (e.g. D'Orazi et al. 2015) where the effects of dilution and thermohaline mixing add to the complexity, can therefore not be used as evidence for an absence of an anticorrelation of the initial Li–Na abundances. Stellar evolution models including all the relevant internal processes are thus urgently needed to explain the Li data in GC stars all along their evolution and to definitively assess the validity of an initial Li–Na anticorrelation right after cluster formation.

4.4 The final fate of the SMS

In practice, our model requires the conveyor belt mechanism to cease, before the SMS releases He-burning products or supernova ejecta. At this point we can only speculate why this should be the case. One possibility is that gas accretion into the cluster stops during the H-burning phase. The gas that remains in the cluster accretes on to the stars and once the cluster is gas-free, stellar winds will no longer be bound by the cluster, but spread their material on a larger scale.

Strongly depending on metallicity and mass-loss, black holes of up to $280\,{\rm M}_\odot$ have been proposed in the literature for stars up to $350\,{\rm M}_\odot$ (Spera & Mapelli 2017). It is hence not inconceivable that an intermediate mass black hole (IMBH) of the order of $10^3\,{\rm M}_\odot$ might result as the remnant of the SMS. It is equally well possible that the SMS is completely disrupted by a pair-instability supernova after sufficient mass-loss (e.g. Yungelson et al. 2008).

Although there is a lot of debate on whether IMBHs are present in GCs (see e.g. Noyola, Gebhardt & Bergmann 2008; Lützgendorf et al. 2011 versus Anderson & van der Marel 2010; Lanzoni et al. 2013; Zocchi, Gieles & Hénault-Brunet 2017; Gieles et al. 2018), an upper limit of $10^3\,{\rm M}_\odot$ is currently allowed by the *N*-body models of Milky Way GCs of Baumgardt (2017). However, we note that clusters form with high densities in our model, such that a small black hole can grow to IMBH masses via stellar collisions on a Gyr time-scale (Giersz et al. 2015). A better understanding of the remnant masses in combination with improved constraints on IMBHs in GCs hence have the potential to rule out the presence of SMSs in proto-GCs.

4.5 Discreteness

In the majority of clusters the main sequence is unimodal, and broadened, but the most massive GCs display two or more distinct main sequences, which implies that there the He abundances are discrete (e.g. Piotto et al. 2015, and references therein). In this section, we suggest two ideas that could lead to discrete He abundances in the SMS-enrichment model. An increase in the He abundance in more massive GCs may result from the (relative) longevity of the contraction phase in massive GCs, resulting in more massive SMSs. More massive SMSs have shorter He production time-scales ($\tau_{\rm He} \lesssim$ Myr) and will therefore produce more He in a fixed time. This, however, only explains why ΔY increases with GC mass, but not why it is bimodal. The multimodality may be understood by considering the He production in the SMS as a function of time. As the SMS grows, Y goes up and $\dot{m}_{\rm wind}$ increases, because $\dot{m}_{\rm wind} \propto \mu^2$ and because $\dot{m}_{\rm wind} \propto m_{\rm SMS}^{0.75-1.5}$ (see Section 3.3). These two effects lead to an increase of the He production rate and the He release rate with time. It remains to be demonstrated whether this material is also efficiently accreted on the low-mass stars, but it provides a first step to understanding a bimodality.

The arguments above cannot be used to understand the presence of more than two main sequences. For this, we need to relax our assumption of monolithic GC formation with a single SMS. In

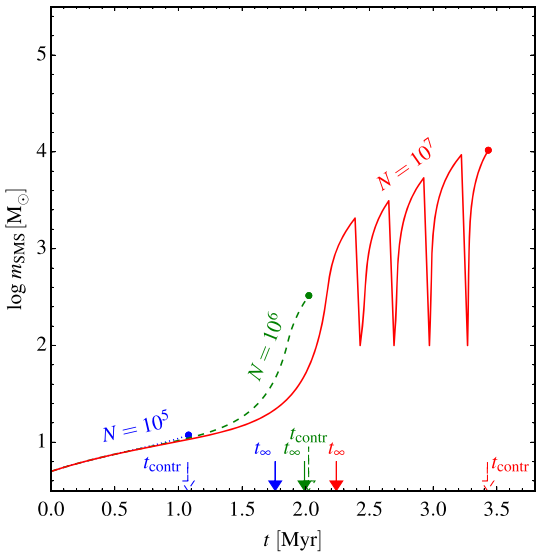

Figure 5. As Fig. 2, but now including the effect of the gravitational instability due to the high radiation pressure (Thompson 2008). For $m_{\rm SMS} > 10^3\,{\rm M}_\odot$, we assume that the SMS fragments and leaves behind a core of $100\,{\rm M}_\odot$ after $10\,\tau_{\rm KH}$ have elapsed. The SMS in the most massive cluster ($N = 10^7$) lives long enough to be affected by this, while the SMS in the smaller clusters never reaches the critical mass and evolutionary phase.

reality, GC formation is hierarchical (see e.g. Krumholz & Bonnell 2007; Offner, Klein & McKee 2008; Sabbi et al. 2012; Smilgys & Bonnell 2017) and massive GCs form from the merger of several smaller stellar clumps. If the total GC mass is large enough, it is possible that more than one of the sub-clumps are massive enough to form their own SMS, each providing material with different levels of enrichment (depending on the mass of the clump), which then form a cluster with distinct levels of chemical enrichment via dry mergers. Also, numerical models of collisional runaway formation of SMSs have shown that a high primordial binary fraction can result in more than one SMS (Gürkan, Fregeau & Rasio 2006).

An alternative route to discreteness – which may also operate in conjunction with the subclustering – is the slow-Jeans instability that SMSs may undergo as the result of their high radiation pressure (Thompson 2008). This instability and subsequent fragmentation develops on a Kelvin–Helmholtz time-scale, $\tau_{\rm KH}$. To see whether this instability may be important for the time-scales we consider here, we consider again our model from Fig. 2 and now assume that this instability is important for SMSs with masses in excess of $10^3\,{\rm M}_\odot$. We assume that after $10\,\tau_{\rm KH}$ the SMS fragments and leaves a core of $100\,{\rm M}_\odot$. The factor of 10 is based on the fact that $\tau_{\rm KH}$ is about 10 times longer in the core compared to the surface (see fig. 3 in Denissenkov & Hartwick 2014). After the fragmentation the SMS can grow again via stellar collisions. In Fig. 5, we show the result of this model. The SMS in the most massive cluster undergoes several 'restarts', while in the smaller cluster there is not enough time for the instability to develop because the SMS does not exceed $10^3\,{\rm M}_\odot$. The pollution of the intracluster medium halts until the SMS becomes massive enough again to blow a strong wind, with higher helium abundance than before the instability, thereby creating a distinct population. As long as the cluster is dense enough to re-grow the SMS via collisions, this process can repeat several times (see Fig. 5). Because of our limited understanding of this instability, this idea for realizing discreteness is speculative.

We therefore prefer the stellar wind argument above that can explain bi-modal He abundances and the stellar subclustering to create more than two populations. Combined with the fact that we expect the SMS to be able to form sufficient amounts of He (see Section 4.3.2), we conclude that the observed discreteness of MSPs is not an obstacle to further progress and that the SMS formation provides promising possibilities.

4.6 Age dependence

As mentioned in Section 1, there are clusters with ages as young as 2 Gyr in the Magellanic Clouds displaying MSPs in the form of N spreads. There are no conditions in our model that are unique to the early Universe, because the threshold for multiple population formation is set by N and $\dot{M}$. The latter is likely to be higher in gas-rich environments, making the early Universe conditions favourable for the formation of SMSs in GCs, but our model does not restrict MSPs to GCs that form in this epoch. There are no Galactic open clusters with similar ages and masses to see whether the MSPs feature is unique to the Magellanic Clouds, or in fact is a common feature among star clusters with similar ages and masses. One possible explanation for the presence of MSPs in relatively young clusters in the Magellanic Clouds is that dwarf irregular galaxies have long gas-consumption time-scales, resulting in gas-rich galactic environments at relatively low redshift.

It is also important to keep in mind that a SMS is not required to produce N (nor Na) enrichment (e.g. Prantzos et al. 2017, and reference therein). It may be possible that material from FRMSs (Decressin et al. 2007a; Krause et al. 2013) or very massive stars (10^2–$10^3\,{\rm M}_\odot$; Vink 2018), enriched in N and Na, cools when it interacts with cold, pristine gas and accretes on the low-mass stars, in a low-density cluster. More details on the mass budget of the N enrichment are required to assess this idea.

4.7 Cluster structure

One of the implications of this GC formation model is that GCs with MSPs form with very high densities and with a nearly constant $R_{\rm h}$, or massive clusters being even slightly smaller than low-mass clusters after a few Myr (see Fig. 3). An inverted M–$R_{\rm h}$ relation, or nearly constant $R_{\rm h}$ is indeed found for young massive clusters (e.g. Kissler-Patig, Jordán & Bastian 2006; Portegies Zwart, McMillan & Gieles 2010). Old GCs have larger $R_{\rm h}$ than predicted by our model, but a direct comparison cannot be made because the present-day masses and radii are strongly affected by dynamical evolution. In fact, the properties of nearly all Milky Way GCs are affected by relaxation driven evolution (Hénon 1961; Gieles et al. 2011), which means that their present-day $R_{\rm h}$ are almost independent of their initial $R_{\rm h}$. We can therefore only conclude that the present-day $R_{\rm h}$ of GCs does not exclude high initial densities. From models of the radius distribution of GCs, Alexander & Gieles (2013) conclude that high initial densities are preferred. Also, support for very high initial densities of GCs comes from dynamical Monte Carlo models of individual GCs (e.g. Giersz & Heggie 2009, 2011) and the Milky Way GC population (Askar et al. 2017). Clusters with $\tau_{\rm rh}$ much longer than their ages have most likely not formed very dense. The low-density, intermediate age SMC cluster Lindsay 1 has MSPs. Glatt et al. (2011) show that $\tau_{\rm rh} \simeq 8$ Gyr, i.e. very similar to its age. If this cluster has not undergone any processes that have inflated its radius in addition to two-body relaxation (i.e. cluster mergers, tidal interaction, etc.), it is difficult to understand the MSPs of this cluster with our model. However, we recall that a SMS is not required to

produce N, and it may be that winds of O-stars or very massive stars were trapped in low-density clusters (see Section 4.6 and Vink 2018).

4.8 SMS radius

In Section 3.4, we show that the amount of polluted material that is released is sensitive to the uncertain mass–radius relation of SMSs. The radius of the SMS, $r_{\rm SMS}$, is controlled by the index δ in the mass–radius relation (equation 5). For $m_{\rm SMS} = 10^4\,{\rm M}_\odot$ we obtain a radius of $r_{\rm SMS} \simeq 300\,{\rm R}_\odot (3000\,{\rm R}_\odot)$ for $\delta = 0.5(1)$, which is larger than the radii of the SMS in the models of Denissenkov & Hartwick (2014) (few$\times\ 10^2\,{\rm R}_\odot$, Denissenkov private communication), but the exact structure of the SMS is sensitive to many of the assumptions that have to be made and models with larger $r_{\rm SMS}$ exist. For example, the models of SMSs with masses up to $10^3\,{\rm M}_\odot$ and solar abundance of Yungelson et al. (2008) show a nearly linear mass–radius relation (i.e. $\delta = 1$), which would have $r_{\rm SMS} \simeq 10^3\,{\rm R}_\odot$ when extrapolating their mass–radius relation to $m_{\rm SMS} = 10^4\,{\rm M}_\odot$. Ishii, Ueno & Kato (1999) find even larger radii for stars of solar abundance and $10^3\,{\rm M}_\odot$. These large radii may be the result of the high metallicity, and more metal-poor stars are likely smaller. We note that the radii we explored here are all below the maximum radius that is set by the Hayashi limit, which is defined by $T_{\rm eff} \simeq 3000\,{\rm K}$ and is due to the steep drop in H^- opacity with temperature. For the luminosity of equation (6), we find that this maximum radius is $r_{\rm SMS} \simeq 6.2 \times 10^3\,{\rm R}_\odot\,(m_{\rm SMS}/100\,{\rm M}_\odot)^{1/2}$. The amount of polluted material produced is sensitive to $r_{\rm SMS}$, therefore it will be critical to improve in the near future our understanding of the structure of SMSs up to $\sim 10^5\,{\rm M}_\odot$, including rotation, general relativistic effects, and disequilibrium evolution as the result of collisions.

4.9 Disruptive collisions

In our model, we have not included the effect of mass-loss following a collision. In SPH models of massive star collisions, Gaburov, Lombardi & Portegies Zwart (2008) find that less than 10 per cent of the mass is ejected from the collision product, and even lower for higher mass ratios. However, head-on collisions, with high relative velocity, could be disruptive for both stars (Freitag & Benz 2005). Because the SMS has a large radius, even grazing collisions could be disruptive and shed parts of the envelope. This may reduce the growth of $m_{\rm SMS}$, and liberate additional material from the SMS to pollute the protostars.

Collisions are also more disruptive if gravitational focusing is unimportant. However, for our adopted mass–radius relation, the escape velocity from the surface of the SMS is $v_{\rm esc,\,SMS} \simeq 1100\,{\rm km\,s^{-1}} (m_{\rm SMS}/100\,{\rm M}_\odot)^{(1-\delta)/2}$, such that for $\delta \leq 1$, the escape velocity is always larger than $1100\,{\rm km\,s^{-1}}$ and we are always in the regime that gravitational focusing is important and little mass is lost in collisions (Freitag & Benz 2005).

4.10 Observational predictions

Here, we provide several predictions that can be used to test the SMS formation model and the associated GC self-enrichment scenario presented in this paper.

(i) Star formation at high redshift: Depending on the mass–radius relation (i.e. the value of δ), the outer parts of the SMS could be relatively cold. For $\delta = 0.5$ we estimate $T_{\rm eff} = 43\,{\rm kK}$, and for $\delta = 1$ we estimate $7.6 \lesssim T_{\rm eff}/{\rm kK} \lesssim 13.6$, for $10^5 \gtrsim m_{\rm SMS}/{\rm M}_\odot \gtrsim 10^4$ (note that more massive $m_{\rm SMS}$ implies cooler $T_{\rm eff}$ for $\delta > 0.5$). Therefore, the SMS could be almost as cool as red supergiants, which normally appear in stellar populations of 10–15 Myr. Combined with the strong wind mass-loss, we expect to see P Cygni profiles or emission lines in a spectrum with relatively low temperatures (e.g. H α or Ca II in emission depending on the effective temperature). The Ca II features could be comparable to those exhibited by the coolest LBVs or by the peculiar SN 2002bu and SN 2010dn in their late and coolest phases (e.g. Smith et al. 2011). Because of the high luminosity of the SMS ($10^{9-10}\,{\rm L}_\odot$; Denissenkov & Hartwick 2014), these spectroscopic features may be observable in star-forming regions at a redshift of $z \gtrsim 2$ ($V \lesssim 26$ mag for $10^{10}\,{\rm L}_\odot$) with future 30-metre class telescopes and the *James Webb Space Telescope*. With existing facilities these features could be looked for in gravitationally lensed star-forming galaxies (e.g. Sobral et al. 2015), where individual clumps can be resolved (e.g. Vanzella et al. 2017). These spectroscopic features in the optical should be visible in combination with signs of inflow of cold molecular gas, potentially observable with *ALMA*. The spectroscopic feature of the cool SMS will be super imposed on stellar populations features from very young stellar populations ($\lesssim$3 Myr), such as hot O-stars in excess of $100\,{\rm M}_\odot$ that may display He II λ1640 in emission. Strong He II λ1640 emission lines were found in gravitationally lensed star-forming regions at redshifts $z \simeq 6{-}7$ (e.g. Sobral et al. 2015), which were also attributed to Population III stars (Schaerer 2003). In the resolved starburst cluster R136 in 30 Doradus, this emission line is entirely produced by the seven stars with masses $\gtrsim 100\,{\rm M}_\odot$ (Crowther et al. 2016), which have strong, but slow winds because of their near Eddington luminosity, resulting in narrow emission lines (Gräfener & Vink 2015). A discussion on the different contributions to He II, and other lines, is presented in Senchyna et al. (2017). Unfortunately, the high gas densities may obscure the SMS and stellar populations for a significant fraction of their life, making it impossible to make solid predictions for the number of SMSs that should be observable.

(ii) GC kinematics: Because the SMS grows via stellar collisions, the angular momentum of the star builds up in a random walk process, and the SMS will therefore have a random spin direction with respect to the angular momentum of the pristine population, and a rotation velocity of order $\sim 100\,{\rm km\,s^{-1}}$. Because of angular momentum conservation, this rotational velocity becomes negligible once the wind reaches $\sim$1 pc. Assuming that the stars that accrete more processed material than their seed mass inherit the angular momentum of the SMS wind, we expect the stars with most extreme abundances to have low streaming motions in the cluster, and could be counter-rotating or corotating with the pristine population. Also, the spin axes of the pristine population and (extreme) polluted populations do not need to be aligned. The prediction for the low orbital spin for the polluted stars is opposite to that of the MGMs, because there the polluted population forms out of material from a first population, and when the material cools to form new stars, the rotational velocity goes up because of angular momentum conservation. As a result, on the MGMs the angular momentum vectors are aligned. In the FRMS scenario of Krause et al. (2013), the second generation of stars is formed as companions in the decretion discs of massive first-generation stars and hence share their kinematics. In the early disc accretion model of Bastian et al. (2013) the polluted population is expected to rotate slower (Hénault-Brunet et al. 2015), but have aligned spin axes. In M13, Cordero et al. (2017) find that the polluted population rotates faster, and the relative angle between the spin axes is between 0 and 45 deg. Contrary to M13, in ω Cen the polluted population rotates slower than the pristine

population (Bellini et al. 2018). This cluster-to-cluster variation of the relative rotation speeds of the two populations is expected in our model, but further studies of differential rotation of multiple population in GCs are needed to shed light on the magnitude and orientation of the orbital angular momentum vectors of the different populations. Several studies have found that the polluted stars have more radially anisotropic orbits (see Richer et al. 2013 for 47 Tuc, Bellini et al. 2015 for NGC 2808 and Bellini et al. 2018 for ω Cen). In our model we expect this to be the case, because the polluted stars are initially more centrally concentrated, and during their evolution they are expected to be scattered to wider, radial orbits (Hénault-Brunet et al. 2015). However, this is not a unique kinematic signature, because in every other scenario the polluted stars are also initially more centrally concentrated.

(iii) [Fe/H] dependence: At lower [Fe/H] the SMS is hotter (for a given $m_{\rm SMS}$). This predicts that the extent of the Mg–Al anticorrelation is larger at lower [Fe/H]. Because we also find a strong (super-linear) correlation between $m_{\rm SMS}$ and cluster mass, we expect preferentially the massive and metal-poor GCs to contain more pronounced Mg–Al anticorrelations. Indications for such a dependence of the Mg–Al anticorrelation on both M and [Fe/H] were found in the Galactic GCs by Carretta et al. (2009b) and Pancino et al. (2017). A M and [Fe/H] dependence was also found for the slope of the O–Na anticorrelation (Carretta et al. 2009a), in the sense that a shallower slope (i.e. a lower minimum O abundance and maximum Na abundance) was found for more massive, metal-poor GCs. A shallower slope of the O–Na anticorrelation is what is expected from the yields of more massive SMSs (see fig. 1 of Denissenkov et al. 2015) and the results of Carretta et al. (2009a) therefore supports the fact that massive, metal-poor GCs had more massive SMSs. However, we caution that there are other metallicity effects: the wind mass-loss rates increase with [Fe/H], which may imply higher $m_{\rm SMS}$ at lower [Fe/H] and work in the same direction as the temperature dependence. But this also predicts a higher fraction of polluted material in more metal-rich GCs, while Milone et al. (2017) find no such correlation. However, we note that metal-rich stars are larger, and a larger cross-section leads to a higher collision rate, working in the opposite direction (more massive SMS at higher [Fe/H] and therefore higher $\dot{m}_{\rm wind}$). The sensitivity to our poorly constrained model parameters δ and η (see Fig. 3), which may both depend on [Fe/H], complicates the discussion on [Fe/H] dependence.

(iv) GCs without MSPs: All clusters with MSPs should have $\tau_{\rm rh} \lesssim$ Age. It would therefore be interesting to look for signatures of MSPs, in the extended clusters in M31 (e.g. Huxor et al. 2005) or some of the low-density outer-halo clusters in the Milky Way, such as Crater or the Palomar clusters with $\tau_{\rm rh} >$ Age. It would in particular be interesting to look for the Mg–Al anticorrelation in these clusters, because this cannot be produced with ordinary O-stars and therefore a SMS is required and it is not expected to form in these clusters in our model.

(v) Young massive clusters: Finally, it may be worthwhile to look for low-redshift analogues of this GC formation model. Signatures of high gas inflow rates in star-forming regions in nearby starburst galaxies have been reported (Turner et al. 2015; Oey et al. 2017). If the mass accretion rates are high enough, these regions may harbour an obscured SMS.

5 CONCLUSIONS

We present a model for the concurrent formation of SMSs and GCs, and use this to explain the abundance anomalies that are observed in old, Fe-normal GCs, and intermediate aged massive star clusters ($\gtrsim$2 Gyr; Martocchia et al. 2018). In our model, the SMS forms via stellar collisions, which are triggered by a contraction of the proto-GC following gas accretion on to its member protostars. A formation mechanism in which dense, massive clusters result from gas inflow and hierarchical cluster assembly is supported by both hydrodynamical simulations of globally collapsing molecular clouds (Vázquez-Semadeni et al. 2017) and observations (e.g. Longmore et al. 2014; Walker et al. 2016)[8]. The formation of SMSs via stellar collisions has been addressed with numerical simulations (Portegies Zwart & McMillan 2002; Portegies Zwart et al. 2004; Freitag et al. 2006; Katz, Sijacki & Haehnelt 2015; Mapelli 2016; Sakurai et al. 2017), which all conclude that the rate of growth of the SMS is sensitive to the adopted initial density of the cluster. In our model, $m_{\rm SMS}$ is insensitive to the initial cluster density, because the cluster density increases as the result of gas accretion, until two-body relaxation becomes important and reduces the density. The resulting $m_{\rm SMS}$ is therefore only a function of the total number of stars N and the gas accretion rate $\dot{M}$, in the sense that massive clusters ($N \gtrsim 10^6$) experiencing a high accretion rate ($\dot{M} \gtrsim 10^5\,{\rm M}_\odot\,{\rm Myr}^{-1}$) are able to form a SMS before relaxation becomes important.

Because SMSs are convective objects, we argue that the fuelling of pristine material via collisions allows the stars to remain close to their early-main-sequence configuration (i.e. the central temperature remains in the 70–80 MK range and the central He content does not increase, as it would in the absence of collisions). Therefore, we assume that all along the accretion phase the He content of the ejecta remains at low values and that the CNONaMgAl patterns are preserved and similar to the values given by the current models at that phase until the stars succumb to their winds or to the Jeans instability. The corresponding yields of SMSs show excellent agreement with the abundances of anomalous stars in GCs once dilution with pristine gas is accounted for (Denissenkov & Hartwick 2014). The relation we obtain between the mass of the cluster and the maximum mass of the SMS, together with the dependence between the central temperature of the SMS and its mass and metallicity is well supported by the indications of a bivariate relation of the Mg depletion with the Galactic GCs masses and [Fe/H].

Our model provides a scenario for the formation of a SMS, but also for the pollution of the low-mass protostars in the cluster: the SMS wind interacts with the inflowing cold gas, subsequently cools and accretes on to the protostars in the cluster. In our model, we are able to overcome the mass budget problem, since the accumulated mass in SMS winds can supersede the maximum mass of the SMS itself by more than an order of magnitude, because it is continuously rejuvenated with fresh hydrogen by stellar collisions. This avoids the need for cluster birth masses that are more than an order of magnitude larger than the present day GC masses (D'Ercole et al. 2008; Schaerer & Charbonnel 2011; Conroy 2012), which is at tension with UV-luminosity functions of high-redshift star-forming regions (Boylan-Kolchin 2017) and the (low) number of field stars in dwarf galaxies with GCs (Larsen et al. 2012, 2014). More importantly, our model predicts a super-linear relation between the amount of processed material and GC mass, providing an explanation for the

[8]We note that these authors refer to this formation mechanism as the 'conveyor-belt mode', which in their work refers to continuous gas inflow during cluster formation. In our model, this gas inflow is a requirement to activate the conveyor-belt production of hot-hydrogen burning products from the SMS.

observed increase of the fraction of polluted stars and helium with GC mass (Milone et al. 2014, 2017).

In this study, we focused on Fe-simple GCs, and provide a model that gives rise to CNONaMgAl and He variations in a single cluster formation event. It has been shown that each Fe sub-populations in Fe-complex GCs displays CNONaMgAl variations (see Carretta et al. 2010b for M54 and Marino et al. 2011 for ω Cen). A straightforward explanation for this is that each (unrelated) star formation event in the nucleus of a galaxy results in the formation of a SMS, producing the light-element variations for that sub-population. This idea needs to be scrutinized in future models.

Apart from the observational tests we propose in Section 4.10, another important next step is to validate the scaling relations proposed in this work with numerical simulations. Petts & Gualandris (2017) present results of collisional *N*-body simulations in which very massive stars form and rejuvenate via stellar collisions. To test our model, the hydrodynamical effect of gas accretion and stellar wind interaction needs to be combined with such collisional *N*-body simulations. This will allow to increase our understanding of the formation and evolution of the SMS and its host GC and the pollution scenario with the various scaling relations proposed here.

ACKNOWLEDGEMENTS

We thank Alvio Renzini and an anonymous referee for reports that helped to improve the paper. We are grateful to Douglas Heggie, Abbas Askar, and Mirek Giersz for insightful feedback on an earlier version of the paper and discussions on binary heating and IMBH formation. We thank Rob Izzard and Pavel Denissenkov for discussions on the structure and temperature of SMSs, Daniel Schaerer for an insight on the spectroscopic features of SMSs, and Nikos Prantzos for discussions on nucleosynthesis. We thank Jorick Vink for discussions on stellar winds. MG acknowledges financial support from the Royal Society (University Research Fellowship) and the European Research Council (ERC StG-335936, CLUSTERS). VHB acknowledges support from the NRC-Canada Plaskett Fellowship and from the Radboud Excellence Initiative. CC acknowledges support from the Swiss National Science Foundation (SNF) for the Projects 200020-159543 'Multiple stellar populations in massive star clusters – Formation, evolution, dynamics, impact on galactic evolution' and 200020-169125 'Globular cluster archeology'. OA acknowledges support from the Swedish Research Council (grant 2014-5791) and the Knut and Alice Wallenberg Foundation. NB thanks the ERC for support (CoG-646928). We thank the International Space Science Institute (ISSI, Bern, CH) for welcoming the activities of the Team 271 'Massive Star Clusters Across the Hubble Time' (2013–2016; team leader CC). Most of the processing of the results has been done using the PYTHON programming language and the following open source modules: NUMPY,[9] SCIPY,[10] MATPLOTLIB.[11]

REFERENCES

Abel T., Bryan G. L., Norman M. L., 2002, Science, 295, 93
Alexander P. E. R., Gieles M., 2012, MNRAS, 422, 3415
Alexander P. E. R., Gieles M., 2013, MNRAS, 432, L1
Alexander P. E. R., Gieles M., Lamers H. J. G. L. M., Baumgardt H., 2014, MNRAS, 442, 1265
Amard L., Palacios A., Charbonnel C., Gallet F., Bouvier J., 2016, A&A, 587, A105
Anderson J., 2002, in van Leeuwen F., Hughes J. D., Piotto G., eds, ASP Conf. Ser. Vol. 265, Omega Centauri, A Unique Window into Astrophysics. Astron. Soc. Pac., San Francisco, p. 87
Anderson J., van der Marel R. P., 2010, ApJ, 710, 1032
Askar A., Szkudlarek M., Gondek-Rosińska D., Giersz M., Bulik T., 2017, MNRAS, 464, L36
Bahcall J. N., Wolf R. A., 1976, ApJ, 209, 214
Ballesteros-Paredes J., Hartmann L. W., Pérez-Goytia N., Kuznetsova A., 2015, MNRAS, 452, 566
Baraffe I., Chabrier G., Allard F., Hauschildt P. H., 2002, A&A, 382, 563
Bastian N., 2017, in Charbonnel C., Nota A., eds, IAU Symp. Vol. 316, Formation, Evolution, and Survival of Massive Star Clusters, Cambridge University Press, Cambridge, p. 302.
Bastian N., Lardo C., 2015, MNRAS, 453, 357
Bastian N., Lardo C., 2018, ARA&A, preprint (arXiv:1712.01286)
Bastian N., Lamers H. J. G. L. M., de Mink S. E., Longmore S. N., Goodwin S. P., Gieles M., 2013, MNRAS, 436, 2398
Bastian N., Cabrera-Ziri I., Salaris M., 2015, MNRAS, 449, 3333
Baumgardt H., 2017, MNRAS, 464, 2174
Baumgardt H., Makino J., Ebisuzaki T., 2004a, ApJ, 613, 1133
Baumgardt H., Makino J., Ebisuzaki T., 2004b, ApJ, 613, 1143
Bedin L. R., Piotto G., Anderson J., Cassisi S., King I. R., Momany Y., Carraro G., 2004, ApJ, 605, L125
Bellini A. et al., 2015, ApJ, 810, L13
Bellini A. et al., 2018, ApJ, 853, 86
Binney J., Tremaine S., 2008, Galactic Dynamics, 2nd edn. Princeton Univ. Press, Princeton, NJ
Blumenthal G. R., Faber S. M., Flores R., Primack J. R., 1986, ApJ, 301, 27
Bonifacio P. et al., 2007, A&A, 470, 153
Bonnell I. A., Bate M. R., Zinnecker H., 1998, MNRAS, 298, 93
Boylan-Kolchin M., 2017, preprint (arXiv:1711.00009)
Breen P. G., Heggie D. C., 2012, MNRAS, 425, 2493
Breen P. G., Heggie D. C., 2013, MNRAS, 432, 2779
Cabrera-Ziri I. et al., 2015, MNRAS, 448, 2224
Cabrera-Ziri I., Lardo C., Davies B., Bastian N., Beccari G., Larsen S. S., Hernandez S., 2016, MNRAS, 460, 1869
Carretta E. et al., 2009a, A&A, 505, 117
Carretta E., Bragaglia A., Gratton R., Lucatello S., 2009b, A&A, 505, 139
Carretta E., Bragaglia A., Gratton R. G., Recio-Blanco A., Lucatello S., D'Orazi V., Cassisi S., 2010a, A&A, 516, A55
Carretta E. et al., 2010b, A&A, 520, A95
Charbonnel C., 2006, Nature, 442, 636
Charbonnel C., 2016, in Moraux E., Lebreton Y., Charbonnel C., eds, EAS Publ. Ser. Vol. 80 , Stellar Clusters: benchmarks of stellar physics and galactic evolution, EDP Sciences, France. p. 177.
Charbonnel C., Primas F., 2005, A&A, 442, 961
Charbonnel C., Chantereau W., Krause M., Primas F., Wang Y., 2014, A&A, 569, L6
Clarke C. J., Bonnell I. A., 2008, MNRAS, 388, 1171
Cohn H., 1980, ApJ, 242, 765
Conroy C., 2012, ApJ, 758, 21
Cordero M. J., Hénault-Brunet V., Pilachowski C. A., Balbinot E., Johnson C. I., Varri A. L., 2017, MNRAS, 465, 3515
Crowther P. A., Schnurr O., Hirschi R., Yusof N., Parker R. J., Goodwin S. P., Kassim H. A., 2010, MNRAS, 408, 731
Crowther P. A. et al., 2016, MNRAS, 458, 624
Cyburt R. H., Fields B. D., Olive K. A., Yeh T.-H., 2016, Rev. Mod. Phys., 88, 015004
D'Antona F., Mazzitelli I., 1994, ApJS, 90, 467
D'Antona F., Bellazzini M., Caloi V., Pecci F. F., Galleti S., Rood R. T., 2005, ApJ, 631, 868
D'Antona F., Ventura P., Decressin T., Vesperini E., D'Ercole A., 2014, MNRAS, 443, 3302
D'Ercole A., Vesperini E., D'Antona F., McMillan S. L. W., Recchi S., 2008, MNRAS, 391, 825
D'Orazi V. et al., 2015, MNRAS, 449, 4038

[9] http://www.numpy.org
[10] http://www.scipy.org
[11] http://matplotlib.sourceforge.net

Dale J. E., 2017, MNRAS, 467, 1067
Davis O., Clarke C. J., Freitag M., 2010, MNRAS, 407, 381
De Marchi G., Panagia N., Beccari G., 2017, ApJ, 846, 110
de Mink S. E., Pols O. R., Langer N., Izzard R. G., 2009, A&A, 507, L1
Decressin T., Meynet G., Charbonnel C., Prantzos N., Ekström S., 2007a, A&A, 464, 1029
Decressin T., Charbonnel C., Meynet G., 2007b, A&A, 475, 859
Decressin T., Charbonnel C., Siess L., Palacios A., Meynet G., Georgy C., 2009, A&A, 505, 727
Decressin T., Baumgardt H., Charbonnel C., Kroupa P., 2010, A&A, 516, A73
Denisenkov P. A., Denisenkova S. N., 1990, Sov. Astron. Lett., 16, 275
Denissenkov P. A., Hartwick F. D. A., 2014, MNRAS, 437, L21
Denissenkov P. A., Herwig F., 2003, ApJ, 590, L99
Denissenkov P. A., VandenBerg D. A., Hartwick F. D. A., Herwig F., Weiss A., Paxton B., 2015, MNRAS, 448, 3314
Doherty C. L., Gil-Pons P., Lau H. H. B., Lattanzio J. C., Siess L., 2014, MNRAS, 437, 195
Elmegreen B. G., 2017, ApJ, 836, 80
Elmegreen B. G., Efremov Y. N., 1997, ApJ, 480, 235
Fabian A. C., Pringle J. E., Rees M. J., 1975, MNRAS, 172, 15p
Federrath C., 2015, MNRAS, 450, 4035
Forestini M., Charbonnel C., 1997, A&AS, 123
Freitag M., Benz W., 2005, MNRAS, 358, 1133
Freitag M., Gürkan M. A., Rasio F. A., 2006, MNRAS, 368, 141
Gaburov E., Lombardi J. C., Portegies Zwart S., 2008, MNRAS, 383, L5
Gavagnin E., Bleuler A., Rosdahl J., Teyssier R., 2017, MNRAS, 472, 4155
Georgy C. et al., 2013, A&A, 558, A103
Gieles M., Zocchi A., 2015, MNRAS, 454, 576
Gieles M., Baumgardt H., Heggie D. C., Lamers H. J. G. L. M., 2010, MNRAS, 408, L16
Gieles M., Heggie D. C., Zhao H., 2011, MNRAS, 413, 2509
Gieles M., Balbinot E., Yaaqib R. I. S. M., Hénault-Brunet V., Zocchi A., Peuten M., Jonker P. G., 2018, MNRAS, 473, 4832
Giersz M., Heggie D. C., 2009, MNRAS, 395, 1173
Giersz M., Heggie D. C., 2011, MNRAS, 410, 2698
Giersz M., Leigh N., Hypki A., Lützgendorf N., Askar A., 2015, MNRAS, 454, 3150
Glatt K. et al., 2011, AJ, 142, 36
Glebbeek E., Gaburov E., de Mink S. E., Pols O. R., Portegies Zwart S. F., 2009, A&A, 497, 255
Goodman J., 1984, ApJ, 280, 298
Gräfener G., Vink J. S., 2015, A&A, 578, L2
Gräfener G., Owocki S. P., Vink J. S., 2012, A&A, 538, A40
Gruyters P. et al., 2016, A&A, 589, A61
Gürkan M. A., Fregeau J. M., Rasio F. A., 2006, ApJ, 640, L39
Guszejnov D., Hopkins P. F., 2015, MNRAS, 450, 4137
Hairer E., Nørsett S., Wanner G., 1993, Solving Ordinary Differential Equations I: Nonstiff Problems, Solving Ordinary Differential Equations. Springer, Berlin
Hartmann L., Herczeg G., Calvet N., 2016, ARA&A, 54, 135
Heggie D. C., 1975, MNRAS, 173, 729
Heggie D., Hut P., 2003, The Gravitational Million-Body Problem: A Multidisciplinary Approach to Star Cluster Dynamics. Cambridge Univ. Press, Cambridge
Heggie D. C., Hut P., Mineshige S., Makino J., Baumgardt H., 2007, PASJ, 59, L11
Hénault-Brunet V., Gieles M., Agertz O., Read J. I., 2015, MNRAS, 450, 1164
Hennebelle P., Chabrier G., 2008, ApJ, 684, 395
Hénon M., 1961, Ann. Astrophys., 24, 369; English translation: (arXiv: 1103.3499)
Hénon M., 1965, Ann. Astrophys., 28, 62; English translation: (arXiv:1103 .3498)
Hills J. G., 1980, ApJ, 235, 986
Hills J. G., Day C. A., 1976, Astrophys. Lett., 17, 87
Hollyhead K. et al., 2017, MNRAS, 465, L39
Humphreys R. M., Davidson K., 1994, PASP, 106, 1025
Huxor A. P., Tanvir N. R., Irwin M. J., Ibata R., Collett J. L., Ferguson A. M. N., Bridges T., Lewis G. F., 2005, MNRAS, 360, 1007
Ishii M., Ueno M., Kato M., 1999, PASJ, 51, 417
Karakas A., Lattanzio J. C., 2007, PASA, 24, 103
Karakas A. I., Fenner Y., Sills A., Campbell S. W., Lattanzio J. C., 2006, ApJ, 652, 1240
Katz H., Sijacki D., Haehnelt M. G., 2015, MNRAS, 451, 2352
Khalaj P., Baumgardt H., 2015, MNRAS, 452, 924
Kim S. S., Lee H. M., Goodman J., 1998, ApJ, 495, 786
Kim J.-h. et al., 2018, MNRAS, 474, 4232
Kimm T., Cen R., Rosdahl J., Yi S. K., 2016, ApJ, 823, 52
King I. R., 1966, AJ, 71, 64
Kissler-Patig M., Jordán A., Bastian N., 2006, A&A, 448, 1031
Korn A. J., Grundahl F., Richard O., Barklem P. S., Mashonkina L., Collet R., Piskunov N., Gustafsson B., 2006, Nature, 442, 657
Korn A. J., Grundahl F., Richard O., Mashonkina L., Barklem P. S., Collet R., Gustafsson B., Piskunov N., 2007, ApJ, 671, 402
Krause M., Charbonnel C., Decressin T., Meynet G., Prantzos N., Diehl R., 2012, A&A, 546, L5
Krause M., Charbonnel C., Decressin T., Meynet G., Prantzos N., 2013, A&A, 552, A121
Krause M. G. H. et al., 2015, A&A, 578, A113
Krause M. G. H., Charbonnel C., Bastian N., Diehl R., 2016, A&A, 587, A53
Kretschmer K., Diehl R., Krause M., Burkert A., Fierlinger K., Gerhard O., Greiner J., Wang W., 2013, A&A, 559, A99
Kroupa P., 2001, MNRAS, 322, 231
Krumholz M. R., Bonnell I. A., 2009, in G. Chabrier, ed. Structure Formation in Astrophysics, Cambridge University Press, Cambridge
Krumholz M. R., Klein R. I., McKee C. F., Offner S. S. R., Cunningham A. J., 2009, Science, 323, 754
Lamers H. J. G. L. M., Cassinelli J. P., 1999, Introduction to Stellar Winds. Cambridge Univ. Press, Cambridge , p. 452
Langer G. E., Hoffman R., Sneden C., 1993, PASP, 105, 301
Lanzoni B. et al., 2013, ApJ, 769, 107
Lardo C., Bellazzini M., Pancino E., Carretta E., Bragaglia A., Dalessandro E., 2011, A&A, 525, A114
Larsen S. S., Strader J., Brodie J. P., 2012, A&A, 544, L14
Larsen S. S., Brodie J. P., Forbes D. A., Strader J., 2014, A&A, 565, A98
Larsen S. S., Baumgardt H., Bastian N., Brodie J. P., Grundahl F., Strader J., 2015, ApJ, 804, 71
Li H., Gnedin O. Y., Gnedin N. Y., Meng X., Semenov V. A., Kravtsov A. V., 2017, ApJ, 834, 69
Lind K., Primas F., Charbonnel C., Grundahl F., Asplund M., 2009, A&A, 503, 545
Lind K., Charbonnel C., Decressin T., Primas F., Grundahl F., Asplund M., 2011, A&A, 527, A148
Lombardi J. C., Thrall A. P., Deneva J. S., Fleming S. W., Grabowski P. E., 2003, MNRAS, 345, 762
Longmore S. N. et al., 2014, in Beuther H., Klessen R. S., Dullemond C. P., Henning T. , Protostars and Planets VIProtostars and Planets VI. Univ. Arizona Press, Tucson, AZ, p. 291
Lützgendorf N., Kissler-Patig M., Noyola E., Jalali B., de Zeeuw P. T., Gebhardt K., Baumgardt H., 2011, A&A, 533, A36
Maeder A., Meynet G., 2006, A&A, 448, L37
Mapelli M., 2016, MNRAS, 459, 3432
Marino A. F. et al., 2011, ApJ, 731, 64
Martocchia S. et al., 2018, MNRAS, 473, 2688
Meléndez J., Casagrande L., Ramírez I., Asplund M., Schuster W. J., 2010, A&A, 515, L3
Mészáros S. et al., 2015, AJ, 149, 153
Milone A. P., Marino A. F., Piotto G., Bedin L. R., Anderson J., Aparicio A., Cassisi S., Rich R. M., 2012, ApJ, 745, 27
Milone A. P. et al., 2013, ApJ, 767, 120
Milone A. P. et al., 2014, ApJ, 785, 21
Milone A. P. et al., 2015, ApJ, 808, 51
Milone A. P. et al., 2017, MNRAS, 464, 3636
Moeckel N., Clarke C. J., 2011, MNRAS, 410, 2799

Moeckel N., Holland C., Clarke C. J., Bonnell I. A., 2012, MNRAS, 425, 450
Monaco L., Bonifacio P., Sbordone L., Villanova S., Pancino E., 2010, A&A, 519, L3
Mucciarelli A., Carretta E., Origlia L., Ferraro F. R., 2008, AJ, 136, 375
Mucciarelli A., Salaris M., Lovisi L., Ferraro F. R., Lanzoni B., Lucatello S., Gratton R. G., 2011, MNRAS, 412, 81
Muijres L. E., Vink J. S., de Koter A., Müller P. E., Langer N., 2012, A&A, 537, A37
Murray N., Chang P., 2015, ApJ, 804, 44
Nadyozhin D. K., Razinkova T. L., 2005, Astron. Lett., 31, 695
Nardiello D. et al., 2015, MNRAS, 451, 312
Nardiello D. et al., 2018, MNRAS, 477, 2004
Niederhofer F. et al., 2017, MNRAS, 465, 4159
Norris J. E., 2004, ApJ, 612, L25
Noyola E., Gebhardt K., Bergmann M., 2008, ApJ, 676, 1008
Oey M. S., Herrera C. N., Silich S., Reiter M., James B. L., Jaskot A. E., Micheva G., 2017, ApJ, 849, L1
Offner S. S. R., Chaban J., 2017, ApJ, 847, 104
Offner S. S. R., Klein R. I., McKee C. F., 2008, ApJ, 686, 1174
Padoan P., Nordlund Å., 2002, ApJ, 576, 870
Padoan P., Haugbølle T., Nordlund Å., 2014, ApJ, 797, 32
Pancino E. et al., 2017, A&A, 601, A112
Pasquini L., Bonifacio P., Molaro P., Francois P., Spite F., Gratton R. G., Carretta E., Wolff B., 2005, A&A, 441, 549
Paxton B., Bildsten L., Dotter A., Herwig F., Lesaffre P., Timmes F., 2011, ApJS, 192, 3
Paxton B. et al., 2013, ApJS, 208, 4
Petts J. A., Gualandris A., 2017, MNRAS, 467, 3775
Pinsonneault M. H., Charbonnel C., Deliyannis C. P., 2000, in da Silva L., de Medeiros R., Spite M., eds, IAU Symp. Vol. 198, The Light Elements and their Evolution, The Astronomical Society of the Pacific (ASP), USA, p. 74
Piotto G. et al., 2007, ApJ, 661, L53
Piotto G. et al., 2015, AJ, 149, 91
Portegies Zwart S. F., McMillan S. L. W., 2002, ApJ, 576, 899
Portegies Zwart S. F., Baumgardt H., Hut P., Makino J., McMillan S. L. W., 2004, Nature, 428, 724
Portegies Zwart S. F., McMillan S. L. W., Gieles M., 2010, ARA&A, 48, 431
Prantzos N., Charbonnel C., 2006, A&A, 458, 135
Prantzos N., Charbonnel C., Iliadis C., 2007, A&A, 470, 179
Prantzos N., Charbonnel C., Iliadis C., 2017, A&A, 608, A28
Regan J. A., Haehnelt M. G., 2009, MNRAS, 396, 343
Renzini A. et al., 2015, MNRAS, 454, 4197
Rey-Raposo R., Dobbs C., Agertz O., Alig C., 2017, MNRAS, 464, 3536
Richer H. B., Heyl J., Anderson J., Kalirai J. S., Shara M. M., Dotter A., Fahlman G. G., Rich R. M., 2013, ApJ, 771, L15
Rosen A. L., Krumholz M. R., McKee C. F., Klein R. I., 2016, MNRAS, 463, 2553
Sabbi E. et al., 2012, ApJ, 754, L37
Sakurai Y., Yoshida N., Fujii M. S., Hirano S., 2017, MNRAS, 472, 1677
Salaris M., Cassisi S., 2014, A&A, 566, A109
Salpeter E. E., 1955, ApJ, 121, 161
Sandage A., Wildey R., 1967, ApJ, 150, 469
Sbordone L. et al., 2010, A&A, 522, A26
Schaerer D., 2003, A&A, 397, 527
Schaerer D., Charbonnel C., 2011, MNRAS, 413, 2297
Senchyna P. et al., 2017, MNRAS, 472, 2608
Siess L., 2010, A&A, 512, A10
Simioni M., Milone A. P., Bedin L. R., Aparicio A., Piotto G., Vesperini E., Hong J., 2016, MNRAS, 463, 449
Smilgys R., Bonnell I. A., 2017, MNRAS, 472, 4982
Smith N., Li W., Silverman J. M., Ganeshalingam M., Filippenko A. V., 2011, MNRAS, 415, 773
Sobral D., Matthee J., Darvish B., Schaerer D., Mobasher B., Röttgering H. J. A., Santos S., Hemmati S., 2015, ApJ, 808, 139
Spera M., Mapelli M., 2017, MNRAS, 470, 4739
Spite F., Spite M., 1982, A&A, 115, 357
Spitzer L. J., Hart M. H., 1971, ApJ, 164, 399
Stodolkiewicz J. S., 1986, Acta Astron., 36, 19
Suzuki T. K., Nakasato N., Baumgardt H., Ibukiyama A., Makino J., Ebisuzaki T., 2007, ApJ, 668, 435
Szécsi D., Langer N., Yoon S.-C., Sanyal D., de Mink S., Evans C. J., Dermine T., 2015, A&A, 581, A15
Szécsi D., Mackey J., Langer N., 2018, A&A, 612, A55
Thompson T. A., 2008, ApJ, 684, 212
Tout C. A., Livio M., Bonnell I. A., 1999, MNRAS, 310, 360
Turner J. L., Beck S. C., Benford D. J., Consiglio S. M., Ho P. T. P., Kovács A., Meier D. S., Zhao J.-H., 2015, Nature, 519, 331
Vanzella E. et al., 2017, MNRAS, 467, 4304
Vázquez-Semadeni E., González-Samaniego A., Colín P., 2017, MNRAS, 467, 1313
Ventura P., D'Antona F., Mazzitelli I., Gratton R., 2001, ApJ, 550, L65
Ventura P., Di Criscienzo M., Carini R., D'Antona F., 2013, MNRAS, 431, 3642
Vink J. S., 2018, preprint (arXiv:1803.08042)
Vink J. S., de Koter A., Lamers H. J. G. L. M., 2001, A&A, 369, 574
Vink J. S., Muijres L. E., Anthonisse B., de Koter A., Gräfener G., Langer N., 2011, A&A, 531, A132
Walker D. L., Longmore S. N., Bastian N., Kruijssen J. M. D., Rathborne J. M., Galván-Madrid R., Liu H. B., 2016, MNRAS, 457, 4536
Wijnen T. P. G., Pols O. R., Pelupessy F. I., Portegies Zwart S., 2016, A&A, 594, A30
Yong D., Grundahl F., Norris J. E., 2015, MNRAS, 446, 3319
Yungelson L. R., van den Heuvel E. P. J., Vink J. S., Portegies Zwart S. F., de Koter A., 2008, A&A, 477, 223
Zinnecker H., 1982, Ann. N. Y. Acad. Sci., 395, 226
Zocchi A., Gieles M., Hénault-Brunet V., 2017, MNRAS, 468, 4429

This paper has been typeset from a TEX/LATEX file prepared by the author.